การศึกษาเชิงทฤษฎีของโอลิฟิเนชันของสารประกอบคาร์บอนิลเร่งปฏิกิริยาด้วยคอปเปอร์ออกไซด์
พิลลาร์เคลย์

นางสาวลลิตา นามเมือง

วิทยานิพนธ์นี้เป็นส่วนหนึ่งของการศึกษาตามหลักสูตรปริญญาวิทยาศาสตรมหาบัณฑิต
สาขาวิชาปิโตรเคมีและวิทยาศาสตร์พอลิเมอร์
คณะวิทยาศาสตร์ จุฬาลงกรณ์มหาวิทยาลัย
ปีการศึกษา 2553

THEORETICAL STUDY OF OLEFINATION OF CARBONYL COMPOUNDS
CATALYZED BY COPPER OXIDE-PILLARED CLAY

Miss Lalita Nammueng

ศูนย์วิทยทรัพยากร
จุฬาลงกรณ์มหาวิทยาลัย

A Thesis Submitted in Partial Fulfillment of the Requirements
for the Degree of Master of Science Program in Petrochemistry and Polymer Science
Faculty of Science
Chulalongkorn University
Academic Year 2010
Copyright of Chulalongkorn University

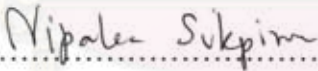|	
Thesis Title	THEORETICAL STUDY OF OLEFINATION OF CARBONYL COMPOUNDS CATALYZED BY COPPER OXIDE-PILLARED CLAY
By	Miss Lalita Nammueng
Field of study	Petrochemistry and Polymer Science
Thesis Advisor	Nipaka Sukpirom, Ph.D.
Thesis Co-Advisor	Associate Professor Vithaya Ruangpornvisuti, Dr.rer.nat.

Accepted by the Faculty of Science, Chulalongkorn University in Partial Fulfillment of the Requirements for the Master's Degree
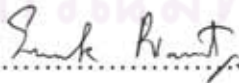
.... Dean of the Faculty of Science

(Professor Supot Hannongbua, Dr.rer.nat.)

THESIS COMMITTEE

.... Chairman

(Professor Pattarapan Prasassarakich, Ph.D.)

.... Thesis Advisor

(Nipaka Sukpirom,Ph.D.)

.... Thesis Co-Advisor

(Associate Professor Vithaya Ruangpornvisuti, Dr.rer.nat.)

.... Examiner

(Assistant Professor Somsak Pianwanit, Ph.D.)

.... External Examiner

(Akapong Suwattanamala, Ph.D.)

ลลิตา นามเมือง : การศึกษาเชิงทฤษฎีของโอลิฟิเนชันของสารประกอบคาร์บอนิลเร่ง
ปฏิกิริยาด้วยคอปเปอร์ออกไซด์พิลลาร์เคลย์. (THEORETICAL STUDY OF
OLEFINATION OF CARBONYL COMPOUNDS CATALYZED BY COPPER OXIDE-
PILLARED CLAY) อ. ที่ปรึกษาวิทยานิพนธ์หลัก : อ.ดร.นิปกา สุขภิรมย์, อ. ที่ปรึกษา
วิทยานิพนธ์ร่วม : รศ.ดร.วิทยา เรืองพรวิสุทธิ์, 82 หน้า.

ศึกษากลไกของปฏิกิริยาโอลิฟิเนชันของสารประกอบ 4–chlorobenzaldehyde เพื่อ
สังเคราะห์ 1–(2,2–dichlorovinyl)–4–chlorobenzene, 3–chlorobenzaldehyde เพื่อสังเคราะห์
1–(2,2–dichlorovinyl)–3–chlorobenzene, 4–bromobenzaldehyde เพื่อสังเคราะห์ 1–(2,2–
dichlorovinyl)–4–bromobenzene, 3–bromobenzaldehyde เพื่อสังเคราะห์ 1–(2,2–
dichlorovinyl)–3–bromobenzene, และ benzaldehyde เพื่อสังเคราะห์ 1–(2,2–dichlorovinyl)–
benzene โดยใช้คอปเปอร์ออกไซด์พิลลาร์เคลย์เป็นตัวเร่งปฏิกิริยา ณ อุณหภูมิ 298 เคลวิน ด้วย
วิธี B3LYP/LanL2DZ พบว่ากลไกการเกิดปฏิกิริยาเหล่านี้ประกอบด้วย 4 ขั้นตอน คือ (1)
precursor formation, (2) dehydrodenitrogenation, (3) chlorination และ (4) recovery
process ค่าพลังงาน สมบัติทางเทอร์โมไดนามิกส์ ค่าคงที่อัตราเร็วและค่าคงที่สมดุลของปฏิกิริยา
ทุกขั้นตอน หาได้จากการคำนวณ

สาขาวิชา ปิโตรเคมีและวิทยาศาสตร์พอลิเมอร์ ลายมือชื่อนิสิต...................................
ปีการศึกษา........................2553........................ ลายมือชื่อ อ.ที่ปรึกษาวิทยานิพนธ์หลัก................
ลายมือชื่อ อ.ที่ปรึกษาวิทยานิพนธ์ร่วม................

#5172423123: PETROCHEMISTRY AND POLYMER SCIENCE PROGRAM

KEYWORDS: COPER OXIDE–PILLARED CLAY / OLEFINATION/ DFT

LALITA NAMMUENG: THEORETICAL STUDY OF OLEFINATION OF CARBONYL COMPOUNDS CATALYZED BY COPPER OXIDE–PILLARED CLAY THESIS ADVISOR: NIPAKA SUKPIROM, Ph.D., THESIS COADVISOR: ASSOC. PROF.VITHAYA RUANGPORNVISUTI, Dr.rer.nat., 82 pp.

The reaction mechanisms of olefinations of the 4–chlorobenzaldehyde (4CBD) to 1–(2,2–dichlorovinyl)–4–chlorobenzene (DCV4CB), 3–chlorobenzaldehyde (3CBD) to 1–(2,2–dichlorovinyl)–3–chlorobenzene (DCV3CB), 4–bromobenzaldehyde (4BBD) to 1–(2,2–dichlorovinyl)–4–bromobenzene (DCV4BB), 3–bromobenzaldehyde (3BBD) to 1–(2,2–dichlorovinyl)–3–bromobenzene (DCV3BB) and benzaldehyde (BD) to 1–(2,2–dichlorovinyl)–benzene (DCVB) catalyzed by Cu–pillared clay were investigated at 298 K using the B3LYP/LanL2DZ method. The mechanism of these reactions composed of (i) precursor formation, (ii) dehydrodenitrogenation (iii) chlorination and (iv) recovery process was found. The energetics, thermodynamic properties, rate and equilibrium constants of all the reaction steps were obtained.

Field of study: Petrochemistry and Polymer Science Student's signature: ....

Academic year: .... 2010 .... Advisor's signature...............................

Co-Advisor's signature.............................

ACKNOWLEDGEMENTS

First of all, I would like to express my sincere gratitude to advisor Dr. Nipaka Sukpirom and Co-advisor Associate Professor Vithaya Ruangpornvisuti, for their invaluable guidance, understanding, and constant encouragement throughout the course of this research. Their positive attitude contributed significantly to inspiring and maintaining my enthusiasm in the field. I feel proud to be their student.

I would like to sincerely thank Professor Dr. Pattarapan prasassarakich, Assistant Professor Dr. Somsak Pianwanit and Dr. Akapong Suwattanamala for kindly serving on my thesis committee. Their sincere suggestions are definitely imperative for accomplishing my thesis.

My gratitude is absolutely extended to all staffs of the Petrochemistry and Polymer Science, Faculty of Science, Chulalongkorn University, for all their kind assistance and cooperation.

Furthermore, I would like to take this opportunity to thank all members in Supramolecular Chemistry Research Unit for their friendly help, creative suggestions, and encouragement. I had a very good time working with them all.

Finally, I really would like to express my sincere gratitude to my parents and family for their support, love, understanding, and cheering.

CONTENTS

LIST OF FIGURES

LIST OF TABLES

LIST OF ABBREVIATIONS AND SYMBOLS

Å	Angstrom
A	Pre-exponential factor
B3LYP	Beck 3 Lee–Yang–Parr
ba	Borane amine
bp	Borane phosphine
c	Speed of light
CPCM	Conductor–like polarizable continuum model
DFT	Density functional theory
E	Energy
G	Gibbs free energy
H	Enthalpy
$\hat{H}$	Hamiltonian operator
HF	Hartree–Fock
h	Plank's constant
IRC	Intrinsic reaction coordinate
k	Rate constant
k_B	Boltzman's constant
K	Equilibrium constant
LanL2DZ	Los Alamos National Laboratory 2 double Zeta
MO	Molecular orbital
PCM	Polarized continuum model
q	Partition function
q_{rot}	Rotational partition function
q_{trans}	Translational partition function
q_{vib}	Vibrational partition function
q_{elect}	Electronic partition function
R	Gas constant
S	Entropy
STO	Slater type orbital
STQN	Synchronous transit–guided quasi–newton

T	Absolute temperature
TS	Transition state
TST	Transition state theory
ZPE	Zero point energy
ZPVE	Zero point vibration energy
ψ	Wave function
χ	Mulliken electronegativity
κ	Kappa
σ	Rotational symmetry number of the molecule
v_i	Imaginary frequency

CHAPTER I

INTRODUCTION

1.1 Background

Olefination of carbonyl compounds, i.e., the conversion of C=O group into C=C bond has found increasing application in the synthesis of substituted alkenes [1]. The product from the olefination are indeed important in organic synthesis, agrochemical [1], pharmaceutical industries [2, 3], modern organic [4], and other chemical fields [5]. Extensive researches of catalysts have been made to develop a cheap and efficient synthetic methodology for the synthesis of specific product [2]. One of several catalyst used for olefination is montmorillonite clay. Montmorillonite is crystalline hydrous aluminosilicates, classified as phyllosilicates, or layered silicate structure by possessing a layered structure [6]. All layered silicates can form two modular units: a sheet of corner linked tetrahedron and a sheet of edge–linked octahedron. The tetrahedral and octahedral sheets are held together by sharing apical oxygen atom [7]. It occurs abundantly in nature and the unique properties of clays contain high surface area, high sorption, reversible ion–exchange and high acidity [8]. However, generally montmorillonite will be substituted with divalent metal ion in order to improve its properties such as large porosity and high specific surface area, together with the possibility of controlling the textural properties [9]. The material obtained is called "pillared clay" [10]. Pillared clay, from a well–known family of microporous materials prepared by multi–step molecular engineering processes. First, the interlayer cations of a layered swellable clay are exchanged by bulk inorganic polyoxocations, leading to the intercalated clays. In the second step, the intercalated clays are calcined at a moderate temperature, the polyoxocations being transformed into pillars, thus leading to the pillared solids. This step is carried out due to the poor thermal stability of the intercalated clays, which may be considered as intermediate precursors of the final stable pillared clays [9]. A great deal of research has concentrated on the use of copper complexes because of their cheapness and efficiency [11, 12, 13].

1.2 Pillared clay

Clay minerals are crystalline hydrous aluminosilicates, classified as phyllosilicates, or layered silicate structures. Clay minerals occur abundantly in nature and the unique properties of clays contain high surface area, high sorption, reversible ion–exchange and high acidity. Their acidity as both Bronsted and Lewis types has been exploited for catalytic applications through decades. Many organic reactions use clays as an efficient heterogeneous catalyst [8].

Clay minerals possess a layered structure, and their suspension in aqueous solution contains particles with the average diameter of about 2 µm [6]. All layered silicates can form two modular units: a sheet of corner linked tetrahedron and a sheet of edge–linked octahedron. The tetrahedral and octahedral sheets are held together by sharing apical oxygen atoms [7].

In the tetrahedral sheet, the dominant cation is Si^{4+} (as in SiO_2), but Al^{3+} substitutes for it frequently and Fe^{3+} does occasionally. This sheet extends infinitely in two dimensions by each tetrahedron sharing three oxygen atoms with three other tetrahedral to form a hexagonal network. They are arranged in a hexagonal pattern with the basal oxygens linking and the apical oxygens pointing upward in the normal direction to the base.

The octahedral sheet is composed of two planes of close–packed oxygen ions with cation residing at the octahedral sites between two planes. The dominant cation is Al^{3+}, but substituted frequently by Mg^{2+} and occasionally by Fe^{2+} and Fe^{3+}. Connection of the neighboring oxygen ions forms a sheet of edge–linked octahedron as hexagonal network, extending infinitely in two dimensions.

The combinations of basic sheets of clays could be divided into 2 categories, namely the 1:1 layered type (T:O, tetrahedral:octahedral sheet) shown in Figure 1.1 (a) and the 2:1 layered type (T:O:T, tetrahedral:octahedral:tetrahedral sheet) shown in Figure 1.1 (b).

| ○ = Oxygens | ⊙ = Hydroxyls | ● = Aluminnum, iron, megnesium | ● and ○ = Silicon, occasionally aluminum |
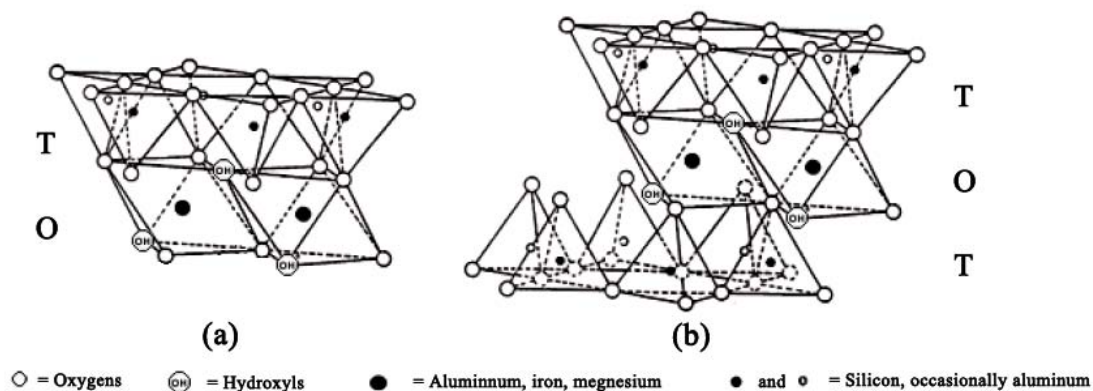
Figure 1.1 Structure of 1:1 layered type (T = Tetrahedral sheet, O = Octahedral sheet) (a), and structure of 2:1 layered type (T = Tetrahedral sheet, O = Octahedral sheet) (b).

Montmorillonite is the main constituent of bentonite, derived by weathering of volcanic ash. In montmorillornite, Mg/Al substitution occurs in the octahedral sheet, with the idealized formula, $(Si_8)(Al_{4-x}Mg_x)O_{20}(OH)_4A_x.nH_2O$ (where A is a monovalent or divalent cation). Montmorillonite can expand by several times of its original volume when it adsorbs water [14].

The insertion of a guest species into the interlayer region of a layered solid is called intercalation, and consequently the layered structure still remains. Intercalation compound can be observed by the XRD pattern, which must unambiguously show an increase in the spacing between adjacent layers, i.e. a change in the basal spacing [10].

Pillaring is the process by which a layered compound is transformed into a pillared compound or a pillared layered solid which is thermally stable micro– and/or mesoporous material with retention of the layer structure. A pillared derivative is distinguished from an ordinary intercalate by virtue of intracrystalline porosity made possible by the lateral separation of the guest specie [10]. Pillared clays, a family of microporous materials, were prepared by the exchange of cations and polyoxocations into the interlayer of swellable clay as shown in Figure 1.2 [15], leading to the intercalated clays. The intercalated clays are calcined, in order to transform polyoxocations into oxide pillars, thus leading to the pillared solids. The possibility of controlling the properties of the pillared solids are performed by varying the type of clay materials (montmorillonite, bentonite, hectorite, etc.) and of intercalating species

(polycations based on Al^{3+}, Si^{4+}, Ti^{4+}, Zr^{4+}, Cr^{3+}, Fe^{3+} or Ca^{2+}, etc) [9]. The resulting material has a high specific surface area and a characteristic porous structure which is of great interest because of its potential application in various fields [16].
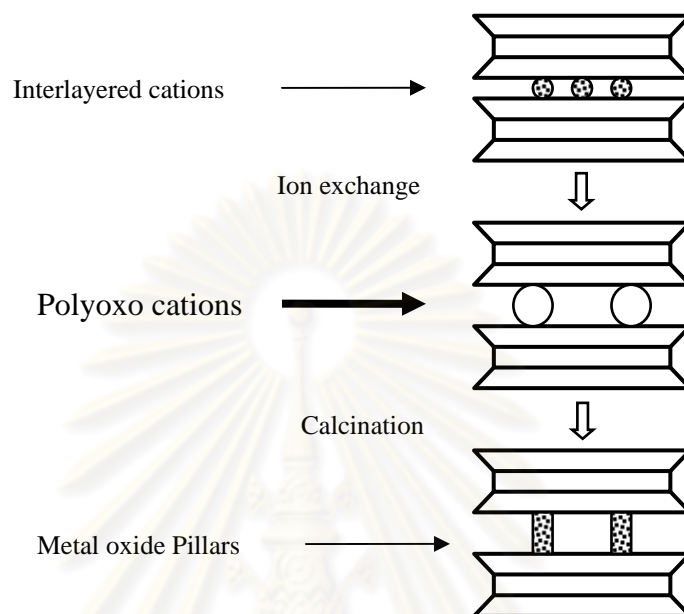
Figure 1.2 Diagram for the preparation of pillared clay compounds.

A pillaring agent is any compound which can be intercalated between adjacent layers of a layered compound. It maintains the interlayer spacing between adjacent layers upon removal of the solvent and induces an experimentally observable pore structure between the layers [10].

1.3 Literature reviews

Extensive theoretical and experimental researches investigated the properties and molecular mechanism for olefination of carbonyl compounds, such as the conversion of C=O group into C=C bond. Many experimental and computational chemistry researches have also been shown to possess appropriate thermodynamic properties to serve as substituted alkenes.

In the 1999, Chatterjee *et al.* [17] had done a research to generate a realistic model for the clay–cation–water system. They used a molecular description of the solvent and clay sheet. They had chosen two clay materials from 2:1 dioctahedral

smectites (1) montmorillonite and (2) beidellite to monitor the effect of negative charge on the location of interlayer cation (Na^+), as the negative charge gets introduced in the clay system from octahedral Al substitution and tetrahedral Si substitution as the case may be (1) and (2), respectively. They used Grand Canonical Monte Carlo (GCMC) simulation to locate the interlayer cation and to calculate the number of interlayer water molecules surrounding the cation (Na^+) for both the clay materials. The results showed that each Na^+ cation is surrounded by five water molecules. The minimum energy conformer obtained from GCMC calculations had been used to generate the cluster model for Local Density Functional (LDF) calculations. The results show the Na^+ cation moves towards the negative center of the clay cluster. It was also observed that Na^+ cation gets more stabilized in montmorillonite in comparison to beidellite.

In the 2003, Nenaidenko *et al.* [1] investigated that Global electrophilicity indices and carbon–halogen bond energies of a wide series of halogen derivatives were calculated in terms of the density functional theory (DFT). The calculated values were used to estimate the reactivity of halogen derivatives under conditions of catalytic olefination. Reactions of N–unsubstituted hydrazones with polyhaloalkanes in the presence of CuCl afforded substituted alkenes. The relation between the structure of polyhaloalkanes and their reactivity was studied using the reaction with 4–chlorobenzaldehyde hydrazone as an example. It was found that increase in the global electrophilicity index and decrease in the C–Hlg bond energy are accompanied by increase in the "olefinating" power of halogen derivatives. In addition, Figure 1.3 illustrates the general mechanism of the catalytic olefination. The reaction is initiated by oxidation of CuCl with halogen–containing compound $CHlg_2XY$; copper(II) thus formed oxidizes hydrazone to give diazoalkane.

The latter undergoes copper–catalyzed decomposition with elimination of nitrogen, leading to copper–carbine complex **A** which is the key intermediate in the catalytic olefination. Further transformations of complex **A** follow two pathways. The reaction with $CHlg_2XY$ results in formation of substituted alkene and regeneration of Cu(II) as catalyst (outer cycle). Aldehyde (ketone) azine is formed as by–product via reaction of the copper–carbene complex with another diazoalkane molecule (inner cycle). Concomitant lowvalence copper compounds should be oxidized with polyhaloalkanes to give products of partial reduction of the latter. Both catalytic cycles, outer and inner, involve the same states of copper catalyst. The ratio of the

hydrazone transformation products, alkenes and azines, depends on the relative contributions of concurrent transformations of complex **A**. In keeping with the proposed mechanism, the "olefinating" reactivity of polyhaloalkanes should be determined by their reaction with complex **A**, which leads to organocopper intermediates **B**, i.e., by their ability to act as electron acceptors, and by the strength of the carbon–halogen bond which is broken as a result of oxidative addition of the copper–carbene complex to the halogen–containing reagent. Increase in the olefinating power of polyhaloalkanes should lead to increase in the yield of the target products (alkenes) and decrease in the yield of by–products (azines), for these reaction pathways compete with each other.
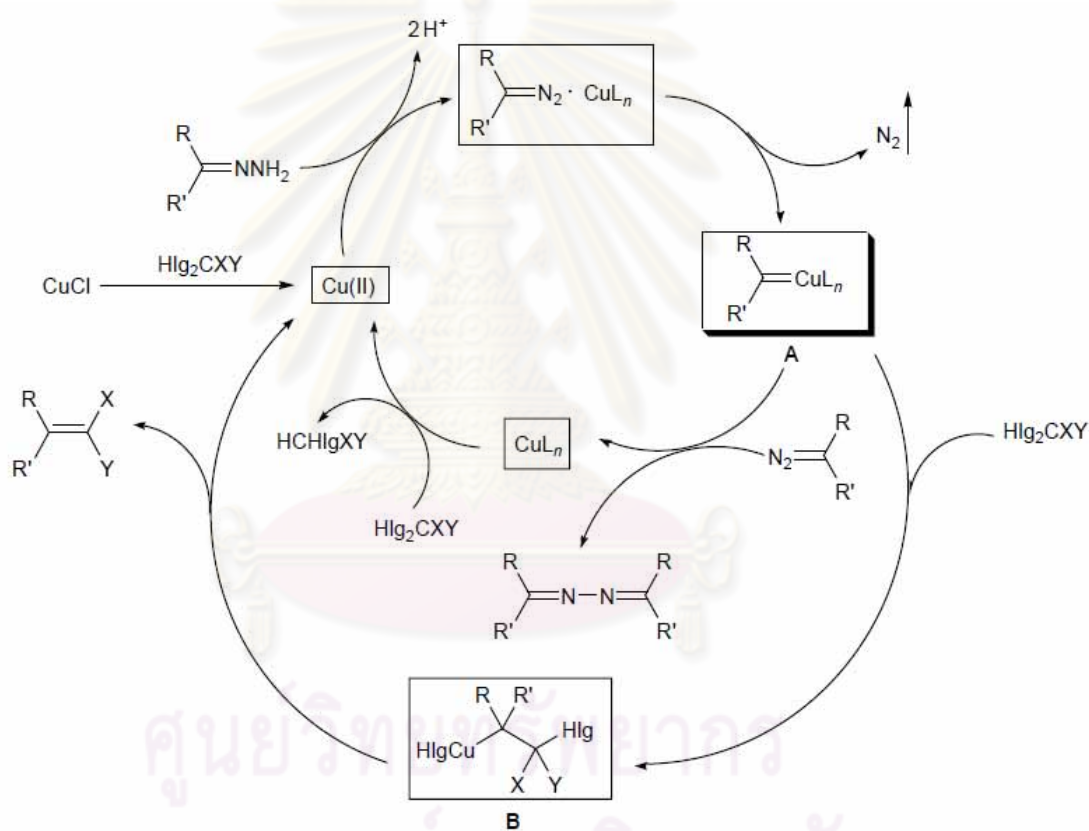
Figure 1.3 Mechanism of the catalytic olefination oxidation of CuCl with halogen–containing compound $CHlg_2XY$.

In the 2005, Shastin *et al.* [18] investigated catalyst nature effect on the catalytic olefination of 4–chlorobenzaldehyde hydrazone by polyhaloalkanes that the best catalysts for the reaction are copper salts. With polyhaloalkanes more active than CCl_4, like CBr_4 and CCl_3Br, the olefination can proceed without catalyst. The catalytic olefination of carbonyl compounds as shown in Figure 1.4 formerly discovered by

their research team aroused a considerable theoretical and practical interest. It was found that the N–unsubstituted hydrazones of carbonyl compounds (both of aldehydes and ketones) treated with polyhaloalkanes in the presence of bases and of copper salts in a catalytic amount were converted into olefins furnishing the corresponding azines as side product. Based on literature and experimental data they suggested a mechanism of the reaction and a catalytic cycle involving a copper–carbene complex as a key intermediate.

R = Ar, Alk; R' = Alk, H; Hlg = Cl, Br; X = F, Cl, Br, H;
Y = F, Cl, Br, CN, CO$_2$Et.
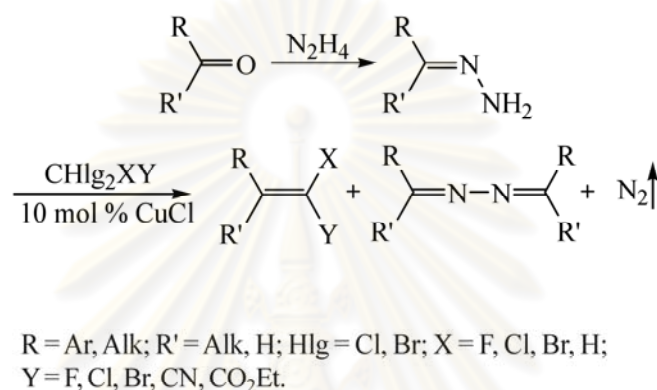
Figure 1.4 Mechanism of the reaction and a catalytic cycle of a copper–carbine complex.

In the 2004, Nenajdenko *et al.* [2] investigated an olefination of hydrazones of aromatic aldehydes by CBrF2–CBrF2 under copper catalysis. In situ prepared aldehydes hydrazones were converted to (3–bromo–2,2,3,3–tetrafluoropropyl)arenes by reaction with CBrF2–CBrF2 in the presence of CuCl. Subsequent elimination of HF by sodium hydroxide resulted in stereospecific formation of fluorocontaining alkenes. Elimination proceeds stereoselectively, only Z–isomers of alkenes are formed. Elimination of two molecules of HF from (3–bromo–2,2,3,3–tetrafluoropropyl)arenes by treatment with potassium tert–butoxide leads to formation of (bromodifluoromethyl)alkynes. As a result a simple and efficient transformation of aromatic aldehydes to range of various fluorinated alkanes, alkenes and alkynes was elaborated.

In the 2005, Joseph *et al.* [19] demonstrated an efficient synthesis of phenyl–(1–phenylethylidene)amine using copper–exchanged montmorillonite clay (Cu K–10). The catalyst was characterized using UV–vis, XRD, BET surface area measurements, pyridine adsorption etc. The XRD and surface area measurement

showed that the structural characteristics of the support montmorillonite K–10 (K–10) are preserved after Cu exchange. The hydroamination of phenyl acetylene with aniline was carried out in toluene under reflux condition in N_2 atmosphere at 393 K. The reaction is highly regio–selective for only Markovnikoff's addition of amine to CC multiple bond and proceeded smoothly to completion. The reaction conditions were optimized to obtain complete conversion with respect to phenyl acetylene. Reaction data showed that the activity of the catalyst in hydroamination reaction is greater at higher reaction temperatures and nonpolar solvents and N_2 pressure promotes the reaction drastically.

In the 2007, An *et al.* [20] had the aim to explore the nature of interaction between organic radicals and paramagnetic ion, unrestricted density functional theory (UDFT) and restricted open shell DFT (RO–DFT) calculations using 6–31G(d) and LANL2DZ basis sets had been performed on the 1:2 complexes of bis(hexafluoroacetylacetonato)copper coordinated with 4–(N–tert–butyl–N–oxyamino)pyridine, complex 1. Structural data revealed by X–ray crystal analysis were used. It was found that the calculated results depend on the selected functionals, model orientation, basis set form and symmetry constraint. The proper chemical models for investigated system are RO–B3LYP, RO–BLYP, RO–PBE, and RO–PBE0.

In the 2008, Ozen *et al.* [11] had done a research in the mechanism of the copper(I)–catalyzed olefin cyclopropanation reaction with dimethyl diazomalonate extensively investigated using the DFT method at B3LYP/6–31G* and BP86/SDD/6–31G* levels. All the possible pathways leading first to a metal carbene and then to the cyclopropane product had been studied with ethene as a model substrate and their energetics demonstrated. Then the suggested mechanisms were applied to a real system: namely, 2,2–dimethyl–4,7–dihydro–1,3–dioxepine.

1.4 Objective

In this study, reaction mechanisms of olefination of halogenobenzaldehyde compounds with hydrazine and carbontetrachloride (CCl_4) to form dihalogenovinyl halogenobenzene compounds catalyzed by copper oxide–pillared clay (Cu–pillared clay) have been studied using the B3LYP/LanL2DZ method. The halogenobenzaldehyde reactants studied in this work are 4–chlorobenzaldehyde

(4CBD), 3–chlorobenzaldehyde (3CBD), 4–bromobenzaldehyde (4BBD), 3–bromobenzaldehyde (3BBD) and benzaldehyde (BD) and their correspounding products are 1–(2,2–dichlorovinyl)–4–chlorobenzene (DCV4CB), 1–(2,2–dichlorovinyl)–3–chlorobenzene (DCV3CB), 1–(2,2–dichlorovinyl)–4–bromobenzene (DCV4BB), 1–(2,2–dichlorovinyl)–3–bromobenzene (DCV3BB) and 1–(2,2–dichlorovinyl)–benzene (DCVB), respectively. Reaction mechanisms of conversions of 4CBD to DCV4CB, 3CBD to DCV3CB, 4BBD to DCV4BB, 3BBD to DCV3BB and BD to DCVB have been investigated. The energetics, thermodynamic properties, rate and equilibrium constants of all the reaction steps have been obtained.

CHAPTER II

THEORETICAL BACKGROUND

2.1 Introduction to quantum mechanics in computational chemistry

Quantum mechanics (QM), also known as quantum physics or quantum theory, is a branch of physics that provides a mathematical description of much of the particle–like and wave–like behavior and interactions of energy and matter departing from classical mechanics at the atomic and subatomic scales. In advanced topics of QM, some of these behaviors are macroscopic and emerge at very low or very high energies or temperatures. The name, coined by Max Planck, derives from the observation that some physical quantities such as the angular momentum of, or more generally the action of, for example, an electron bound into an atom or molecule can be changed only by discrete amounts, or quanta as multiples of the Planck constant, rather than being capable of varying continuously or by any arbitrary amount. An electron bound in an atomic orbital has quantized values of angular momentum while an unbound electron does not exhibit quantized energy levels but the latter is associated with a short quantum mechanical wavelength.

2.2 Density functional theory (DFT) method

The basis for density functional theory (DFT) is the proof by Hohenberg and Kohn that the ground–state electronic energy is determined completely by the electron density ρ. In other words, there exists a one–to–one correspondence between the electron density of a system and the energy. The significance of this is perhaps best illustrated by comparing to the wave function approach. A wave function for an N–electron system contains $3N$ coordinates, three for each electron (four if spin is included). The electron density is the square of the wave function, integrated over N–1 electron coordinates, this only depends on three coordinates, independently of the number of electrons. While the complexity of a wave function increases with the number of electrons, the electron density has the same number of variables, independently of the system size. The "only" problem is that although it has been

proven that each different density yields a different ground–state energy, the functional connection these two quantities is not known. The goal of DFT methods is to design functionals connecting the electron density with the energy.

The foundation for the use of DFT methods in computational chemistry was the introduction of orbitals by Kohn and Sham. The basic idea in the Kohn and Sham (KS) formalism is splitting the kinetic energy functional into two parts, one of which can be calculated exactly, and a small correction term.

2.2.1 The Kohn–Sham energy [21]

The ideal energy is that of an ideal system, a fictitious non–interacting reference system, defined as one in which the electrons do not interact and in which the ground state electron density ρ_r is exactly the same as in our real ground state system, $\rho_r = \rho_0$. The electronic energy of the molecule is the total internal "frozen–nuclei" energy can be found by adding the internuclear repulsions and the 0 K total internal energy by further adding the zero–point energy.

The ground state electronic energy of our real molecule is the sum of the electron kinetic energy, the nucleus–electron attraction potential energies, and the electron–electron repulsion potential energies and each is a functional of the ground–state electron density.

$$E_0 = \langle T[\rho_0] \rangle + \langle V_{ne}[\rho_0] \rangle + \langle V_{ee}[\rho_0] \rangle \tag{2.1}$$

Focussing on the middle term: the nucleus–electron potential energy is the sum over all $2n$ electrons (as with our treatment of *ab initio* theory, we will work with a closed shell molecule which perforce has an even number of electrons) of the potential corresponding to attraction of an electron for all the nuclei A:

$$\langle V_{ne} \rangle = \sum_{i=1}^{2n} \sum_{nuclei A} -\frac{Z_A}{r_{iA}} = \sum_{i=1}^{2n} v(r_i) \tag{2.2}$$

where $v(r_i)$ is the external potential for the attraction of electron i to the nuclei. The density function ρ can be introduce into $\langle V_{ne} \rangle$ by using that

$$\int \psi \sum_{i=1}^{2n} f(r_i) \psi \, dt = \int \rho(r) f(r) dr \qquad (2.3)$$

where $f(r_i)$ is a function of the coordinates of the *2n* electrons of a system and ψ is the total wavefunction from equations (2.2) and (2.3), invoking the concept of expectation value $\langle V_{ne} \rangle = \langle \psi | \hat{V}_{ne} | \rangle \psi$, and since $\hat{V} = V_x$, and get,

$$E_0 = \int \rho_0(r)v(r)dr + \langle T[\rho_0] \rangle + \langle V_{ee}[\rho_0] \rangle \qquad (2.4)$$

that cannot known the function in $\langle T[\rho_0] \rangle$ and $\langle V_{ee}[\rho_0] \rangle$. The Kohn and Sham to introduced the idea of a reference system of non–interacting electrons. Let us to define the quantity $\Delta \langle T[\rho_0] \rangle$ as the deviation of the real kinetic energy from that of the reference system.

$$\Delta \langle T[\rho_0] \rangle \equiv \langle T[\rho_0] \rangle - \langle T_r[\rho_0] \rangle \qquad (2.5)$$

Let us next define $\Delta \langle V_{ee} \rangle$ as the deviation of the real electron–electron repulsion energy from classical charged–cloud coulomb repulsion energy. This classical electrostatic repulsion energy is the summation of the repulsion energies for pairs of infinitesimal volume elements $\rho(r_1)dr_1$ and $\rho(r_2)dr_2$ separated by distance r_{12}, multiplied by one–half. The sum infinitesimals is an integral and so

$$\Delta \langle V_{ee}[\rho_0] \rangle = \langle V_{ee}[\rho_0] \rangle - \frac{1}{2} \iint \frac{\rho_0(r_1)\rho_0(r_2)}{r_{12}} dr_1 dr_2 \qquad (2.6)$$

Actually, the classical charged–cloud repulsion is somewhat inappropriate foe electrons in that smearing an electron out into a cloud forces it to repel itself, as any two regions of the cloud interact repulsively. This physically incorrect electro self–interacting will be compensated for by a good exchange–correlation functional can be written as

$$E_0 = \int \rho_0(r)v(r)dr + \langle T_r[\rho_0] \rangle + \frac{1}{2}\iint \frac{\rho_0(r_1)\rho_0(r_2)}{r_{12}} + \Delta\langle T[\rho_0] \rangle + \Delta\langle V_{ee}[\rho_0] \rangle \qquad (2.7)$$

The sum of the kinetic energy deviation from the reference system and the electron–electron repulsion energy deviation from the classical system is called the exchange–correlation energy, E_{xc}

$$E_{xc}[\rho_0] \equiv \Delta\langle T[\rho_0] \rangle + \Delta\langle V_{ee}[\rho_0] \rangle \qquad (2.8)$$

The $\Delta\langle T \rangle$ term represents the kinetic correlation energy of the electrons and the $\langle \Delta V_{ee} \rangle$ term the potential correlation energy and the exchange energy, although exchange and correlation energy in DFT do have exactly.

2.2.2 The Kohn–Sham equations

The Kohn–Sham (KS) equations [21] are theorem obtained by utilizing the variation principle, which the second Hohenberg–Kohn theorem assures applies to DFT. We use the fact that the electron density of the reference system, which is the same as that of our real system, is given by

$$\rho_0 = \rho_r = \sum_{i=1}^{2n} \left| \psi_i^{KS}(1) \right|^2 \qquad (2.9)$$

where the ψ_i^{KS} are the KS spatial orbital. Substituting the above expression for the orbitals into the energy and varying E_0 with with respect to the ψ_i^{KS} subject to the constraint that these remain orthonormal lead to the KS equations, procedure is similar to that used in deriving the HF equations,

$$\left[-\frac{1}{2}\nabla_i^2 - \sum_{nucleiA} \frac{Z_A}{r_{iA}} + \int \frac{\rho(r_2)}{r_{12}}dr_2 + v_{xc}(1) \right]\psi_i^{KS}(1) = \varepsilon_i^{KS}\psi_i^{KS}(1) \qquad (2.10)$$

where $\in_i^{KS}$ are the KS energy levels and $v_{xc}(1)$ is the exchange correlation potential, arbitrarily designated here for electron number 1, since the KS equations are a set of one–electron equations with the subscript i running from 1 to n, over all the *2n* electron in the system. The exchange correlation potential is defined as the functional derivative of $E_{xc}[\rho_0(r)]$ with respect to $\rho(r)$

$$v_{xc}(r) = \frac{\delta E_{xc}[\rho(r)]}{\delta\rho(r)} \tag{2.11}$$

We need the derivative v_{xc} for the KS equations, and the exchange–correlation function itself for the energy equation. The KS equations can be written as

$$\hat{h}^{KS}(1)\psi_i^{KS}(1) = \varepsilon_i^{KS}\psi_i^{KS}(1) \tag{2.12}$$

The KS operator $\hat{h}^{KS}$ is defined by equation (2.11). The significance of these orbitals and energy levels is considered later, but we note here that in practice they can be interpreted in a similar way to the corresponding HF and extended Huckel entities. Pure DFT theory has no orbitals or wavefunctions; these were introduced by Kohn and Sham only as a way into a useful computational tool, but if we can interpret the KS orbitals and energies in some physically useful way, so much the better.

The KS energy equation is exact: if we knew the density function $\rho_0(r)$ and the exchange–correlation energy functional $E_{xc}[\rho_0]$, it would give the exact energy. The HF energy equation, on the other hand, is an approximation that does not treat electron correlation properly. Similar considerations hold for the KS and HF equations, derived from the energy equations by minimizing the energy with respect to orbitals: even in the basis set limit, the HF equations would not give the correct energy, but the KS equations would, *if we knew the exact exchange–correlation energy functional.* In wavefunction theory we know how to improve on HF–level results: by using perturbational or configuration interaction treatments of electron correlation, but in DFT theory there is as yet no systematic way of improving the exchange–correlation energy functional. It has been said that "while solutions to the

[HF equations] may be viewed as exact solutions to an approximate description, the [KS equations] are approximations to an exact description.

2.2.3 DFT exchange and correlations

The form of E_{XC} is generally unknown and its exact value has been calculated only for a few very simple systems. In the density functional theory, the exchange energy is defined as

$$E_X[\rho] = \left\langle \phi[\rho] \left| \hat{V}_{ee} \right| \phi[\rho] \right\rangle - U[\rho] \tag{2.13}$$

When $U[\rho]$ is the Hartree piece of the columbic potential. The correlation term is defined as the remaining unknown piece of the energy:

$$E_C[\rho] = F[\rho] - T_s[\rho] - U[\rho] - E_X[\rho] \tag{2.14}$$

Due to the definition of $F[\rho]$, the correlation energy consists of two separate contributions:

$$E_C[\rho] = T_C[\rho] + U[\rho] \tag{2.15}$$

when $T_C[\rho]$ and $U_C[\rho]$ are respectively the kinetic contribution and the potential contribution of the correlation energy.

In electronic structure calculations, E_{XC} is the most commonly approximation within the local density approximation or generalized–gradient approximation. In the local density approximation (LDA), the value of $E_{XC}[\rho(r)]$ is approximated by exchange–correlation energy of an electron in homogeneous electron gas of the same density $\rho(r)$, *i.e.*

$$E_{XC}^{LDA}[\rho(r)] = \int \in_{XC} (\rho(r))\rho(r)dr \tag{2.16}$$

The most accurate data for $\in_{XC}(\rho(r))$ is calculated from Quantum Monte Carlo calculation. For the systems with slowly varying charge densities, this approximation generally gives very good results. An obvious approach to improve the LDA, so called generalized gradient approximation (GGA), is to include gradient corrections by making E_{XC} a function of the density and its gradient as shown below

$$E_{XC}^{GGA}[\rho(r)] = \int \in_{XC}(\rho(r))\rho(r)dr + \int F_{XC}[\rho(r),|\nabla\rho(r)|]dr \qquad (2.17)$$

where F_{XC} is a correction chosen to satisfy one or several known limits for E_{XC}. Clearly, there is no unique equation for the F_{XC}, and several functions have been proposed. The development of the improved functions is currently a very active area of research although incremental improvements are likely. It is ambiguous whether the research will be successful in providing the substantial increase in accuracy that is desired.

2.2.4 Hybrid functions

Hybrid functional augment the DFT exchange–correlation energy with a term calculated from Hartree–Fock theory. The Kohn–Sham orbitals are quit similar to the HF orbitals, give an expression, based on Kohn–Sham orbitals, for the HF exchange energy.

$$E_x^{HF} = -\sum_{i=1}^{n}\sum_{j=1}^{n}\left\langle \psi_i^{KS}(1)\psi_i^{KS}(2)\left|\frac{1}{r_{ij}}\right|\psi_j^{KS}(2)\psi_j^{KS}(1)\right\rangle \qquad (2.18)$$

Since the KS Slater determinant is an exact representation of the wavefunction of the noninteracting electron reference system, E_x^{HF} is the exact exchange energy for a system of noninteracting electron with electron density equal to real system.

Including in a LSDA gradient–corrected DFT expression for E_{xc} ($E_{xc} = E_x + E_c$) a weighted contribution of the expression for E_x^{HF} give a FH/DFT exchange–correlation functional, commonly called a hybrid DFT functional. The most popular hybrid functional at present is based on an exchange–energy functional developed by

Becke, and modified Steven *et al.* by introduction of the LYP correlation–energy functional. This exchange–correlation functional, called the Becke3 LYP or B3LYP functional is

$$E_{xc}^{B3LYP} = (1 - a_0 - a_x)E_x^{LSDA} + a_0 E_x^{HF} + a_x E_x^{B88} + (1 - a_c)E_x^{VWN} + a_c E_c^{LYP} \qquad (2.19)$$

Here E_x^{LSDA} is the kind accurate pure DFT LSDA non–gradient–corrected exchange functional, E_x^{HF} is the Kohn–Sham orbitals based HF exchange energy functional, E_x^{B88} is the Becke 88 exchange functional

$$E_x^{B88} = E_x^{LDA} + \Delta E_x^{B88}$$
$$\Delta E_x^{B88} = -\beta\rho^{1/3}\frac{x^2}{1 + 6\beta x \sinh^{-1} x} \qquad (2.20)$$

The β parameter is is determined by fitting to known atomic data and x is a dimension gradient variable. The E_x^{VWN} is the Vosko, Wilk, Nusair function (VWN) can be written

$$E_x^{VWN} = E_x^{LDA}(1 + ax^2 + bx^4 + cx^6)^{1/5}$$
$$x = \frac{|\nabla\rho|}{\rho^{4/3}} \qquad (2.21)$$

which forms part of the accurate functional for the homogeneous electron gas of the LDA and LSDA, and E_c^{LYP} is the LYP correlation functional. The parameters a_0, a_x and a_c are those that give the best fit of the calculated energy to molecular atomization energies. This is thus gradient–corrected hybrid functional [22].

2.3 Basis sets

The approximate treatment of electron–electron distribution and motion assigns individual electrons to one–electron function, termed *spin orbital*. These consist of a product of spatial functions, termed *molecular orbitals (MO)*, $\psi_1(x, y, z)$,

$\psi_2(x,y,z)$, $\psi_3(x,y,z)$, ..., and either α or β spin components. The spin orbitals are allowed complete freedom to spread throughout the molecule. Their exact forms are determined to minimize the total energy. In the simplest level of theory, a single assignment of electron to orbital is made by used ψ as atomic orbital wave function based on the Schrödinger equation for the hydrogen atom. This is not a suitable approach for molecular calculation. This problem can be solved by representing MO as linear combination of basis functions.

In practical calculation, the molecular orbitals $\psi1$, $\psi2$, ..., are further restricted to be linear combinations of a set of N known one–electron function $\phi_1(x,y,z)$, $\phi_2(x,y,z)$, ..., $\phi_N(x,y,z)$:

$$\psi_i = \sum_{\mu=1}^{N} c_{\mu i} \phi_\mu \qquad (2.22)$$

The functions ϕ_1, ϕ_2, ..., ϕ_N, which are defined in the specification of the model, are known as one–electron basis function called basis function. The set of basis functions is called basis set. If the basis functions are the atomic orbitals for the atoms making up the molecule, function in equation 2.23 is often described as the *linear combination of atomic orbitals* (LCAO). There are two types of basis function which commonly used in the electronic structure calculations, *Slater type orbitals* (STO) and *Gaussian type orbitals* (GTO).

The Slater orbitals are primarily used for atomic and diatomic systems where high accuracy is required and semiempirical calculations where all three– and four–center integrals are neglected. The Slater type orbitals have the function form:

$$b = Ae^{-\zeta r} r^{n^*-1} Y_{lm}(\theta, \phi) \qquad (2.23)$$

where parameter n^* and ξ are chosen to make the larger part of the orbitals look like atomic Hartree–Fock orbitals. There are a lot like hydrogen orbitals, but without the complicated nodal structure.

The Gaussian type orbitals can be written in terms of polar or cartesian coordinates:

$$g = x^a y^b z^c e^{-\alpha r^2} Y_{lm}(\theta,\phi) \qquad (2.24)$$

in which *a*, *b*, and *c* are integers and α is a parameter that is usually fixed. Primitive Gaussian function is shown in equation 2.24. Normally, several of these Gaussian functions are summed to define more realistic atomic orbitals basis functions, as shown below:

$$b_\mu = \sum_p k_{\mu p} g_p. \qquad (2.25)$$

The coefficients $k_{\mu p}$ in this expansion are chosen to make the basis functions look as much like Slater orbitals as possible. Slater functions are good approximation to atomic wave functions but required excessive computer time more than Gaussian functions, while single–Gaussian functions are a poor approximation to the nearly ideal description of an atomic wave function that Slater function provides. The solution to the problem of this poor functional behavior is to use several Gaussians to approximate a Slater function. In the simplest version of this basis, n Gaussian functions are superimposed with fixed coefficients to form one–Slater type orbital. Such a basis is denoted STO–nG, and n = 3, 4.

The limit of quantum mechanics involves an infinite set of basis function. This is clearly impractical since the computational expanse of molecular orbital calculations is proportional to the power of the total number of basis functions. Therefore, ultimate choice of basis set size demands on a compromise between accuracy and efficiency. The classification of basis sets is given below.

2.3.1 Minimal basis sets

The minimum basis set [23] is a selected basis function for every atomic orbital that is required to describe the free atom. For hydrogen atom, the minimum basis set is just one *1s* orbital. But for carbon atom, the minimum basis set consisted of a *1s* orbital, a *2s* orbital and the full set of three *2p* orbitals. For example, the minimum basis set for the methane molecule consists of 4 *1s* orbitals, one per hydrogen atom, and the set of *1s*, *2s* and *2p* orbitals described above for carbon. Thus, total basis set comprises of 9 basis functions.

Several minimum basis sets are used as common basis sets especially the STO–nG basis sets because they are available for almost all elements in the periodic table. The most common of minimum basis sets is STO–3G, where a linear combination of three Gaussian type orbitals (GTOs) is fitted to a Slater–type orbital (STO). The individual GTOs are called primitive orbitals, while the combined functions are called contracted functions. For example, the STO–3G basis set for methane consists of a total of 9 contracted functions built from 27 primitive functions. Other commonly uses of STO–nG basis sets are STO–4G and STO–6G where each STO is fitted to 4 and 6 GTOs, respectively.

2.3.2 Scaled orbital by splitting the minimum basis sets

In the early calculation on the hydrogen molecule, it is discovered that the STO *1s* orbitals do not give the best result in the molecular environment when the Schrödinger equation is solved, because electron is attracted to both nuclei rather than just one nucleus. In each molecular orbital, both large and small sets of orbital appear and they are mixed in the ratio that gives the lowest energy. The combination of a large orbital and a small orbital is essentially equivalent to an orbital of intermediate size. The result orbital is a size that best fit for the molecular environment since it is obtained from minimizing the energy. The advantage of this procedure is that the mixing coefficients in the molecular orbitals appear in a linear function. This simple dodge is equivalent to scaling the single minimal basis set orbitals. The minimum basis set can scaled not only the valence orbitals of the minimal basis set (split valence basis set), but also all the orbitals of the minimal basis set (double zeta basis sets).

2.3.2.1 Split the valence orbitals

The split the valence orbitals (split valence basis sets) mean that each valence orbital is spited into two parts, an inner shell and an outer shell. For example, the 3–21G basis set is referred to basis function of the inner shell represented by two Gaussian functions and that of the outer shell represented by one Gaussian function The core orbitals are represented by one basis function and each function composes of three Gaussian functions. The purpose of splitting the valence shell is to give the SCF

algorithm more flexibility in adjusting the contributions of the basis function to the molecular orbitals, achieving a more realistic simulated electron distribution.

2.3.2.2 Split all orbitals

Split orbital (double zeta basis set) is a member of minimum basis set replaced by two functions. In this way both core and valence orbitals are scaled in size. For some heavier atoms, double zeta basis sets may have slightly less than double the number of minimum basis set orbitals. For example, some double zeta basis sets for the atoms Ga–Br have 7 rather than 8 s basis functions, and 5 rather than 6 p basis functions.

The term "*double zeta*" arises from the fact that the exponent in a STO is often referred by the Greek letter "*zeta*". Since it takes two orbitals with different exponents, it is called "*double zeta*". The minimum basis set is "*single zeta*". The normal abbreviation for a double zeta basis set is DZ. It is also quite common to use split valence basis sets where the valence orbitals are spitted into three functions. Basis sets where this is done for all functions are called triple zeta functions and referred to as TZ, TZP, TZ2P etc.

2.3.3 Polarized basis sets

In the discussion on the scaling of the hydrogen orbitals in the H_2 molecule, it is argued that the orbital on one atom in the molecule becomes smaller because of the attraction of the other nucleus. However, it is also clear that the influence of the other nucleus may distort or polarize the electron density near the nucleus. This problem desires orbitals that have more flexible shapes in a molecule than the *s, p, d*, etc., shapes in the free atoms. This is best accomplished by add basis functions of higher angular momentum quantum number. Thus, the spherical *1s* orbital on hydrogen is distorted by mixing in an orbital with p symmetry. The positive lobe at one side increases the value of the orbital while the negative lobe at the other side decreases the orbital. The orbital has overall "moved" sideways. It has been polarized. Similarly, the p orbital can polarize if it mixes in an orbital of d symmetry. These additional basis functions are called polarization functions. The polarization functions are added to the 6–31G basis set as follows:

6–31G* added a set of d orbitals to the atoms in the first and second rows.

6–31G** added a set of d orbitals to the atoms in the first and second rows and a set of p functions to hydrogen.

The nomenclature above is slowly being replaced. The 6–31G* is called 6–31G(d), while the 6–31G** is called 6–31G(d,p). This new nomenclature allows the possibility of adding several polarization functions. Thus 6–31G (3df,pd) added 3 d–type GTOs and 1 f–type GTO and added 1 p–type and 1 d–type function to H.

2.3.4 Diffuse function basis sets

In some cases the normal basis functions are not adequate. This is particular the case in excited states and in anions where the electronic density is spread out more over the molecule. This model has correctly by using some basis functions which themselves are more spread out. This means that small exponents are added to GTOs. These additional basis functions are called diffuse functions. The diffuse functions added to the 6–31G basis set as follows:

6–31+G added a set of diffuse s and p orbitals to the atoms in the first and second rows.

Diffuse functions can be added along with polarization functions also. Some examples of these functions are 6–31+G*, 6–31++G*, 6–31+G** and 6–31++G** basis sets.

2.3.5 Effective core potentials

The use of effective core potentials (ECP) has been a notable success in the molecular orbital calculations involving transition metals. ECP is simply a group of potential functions that replace the inner shell electrons and orbitals that are normally assumed to have minor effects on the formation of chemical bonds. Calculations of the valence electrons using ECP can be carried out at a fraction of the computational cost that is required for an all electron (AE) calculation, while the overall quality of computation does not differ much from the AE calculations. Combined with the use of reliable basis sets, it appears to be a very powerful and economical method for dealing with molecules containing heavy transition metals. Following this approach, the LanL2DZ basis set was employed for geometry optimization. The LanL2DZ basis

sets (a split valence basis) [24] are one of the double basis sets which were used for determining only valence electron in order to be easy in calculation. It contains effective core potential representations of electrons near the nuclei for post–third–row atoms. The reliability of this basis set has been confirmed by the accuracy of calculation results compared with experimental data as well as those from a more expensive all electron basis set.

2.4 Transition state theory and rate constant

Transition state theory (TST) or activated complex theory provides a simple formalism for obtaining thermal rate constant by mixing the important features of the potential energy surface with a statistical representation of the dynamics. In addition to the Born–Oppenheimer approximation, TST is based on three assumptions:

- Classically there exists a surface in phase space that divides it into a reactant region and a product region. It is assumed that this dividing surface is located at the transition state, which is defined as the maximum value on the minimum energy path (MEP) of the potential energy surface that connects the reactant(s) and product(s). Any trajectory passing through the dividing surface from the reactant side is assumed to eventually form products. This is often referred to as the nonrecrossing rule.

- The reactant equilibrium is assumed to maintain a Boltzmann energy distribution.

- Activated complexes are assumed to have Boltzmann energy distributions corresponding to the temperature of the reacting system. These activated complexes are defined as super–molecules having configurations located in the vicinity of the transition state.

In chemistry, transition state theory is a conception of chemical reactions or other processes involving rearrangement of matter as proceeding through a continuous change or "transition state" in the relative positions and potential energies of the constituent atoms and molecules. The theory was first developed by R. Marcelin in 1915, then continued by Henry Eyring and Michael Polanyi (Eyring equation) in 1931, with their construction of a potential energy surface for a chemical reaction, and later, in 1935, by H. Pelzer and Eugene Wigner [25]. Meredith Evans, working in coordination with Polanyi, also contributed significantly to this theory.

TST assumes that a reaction proceeded from one energy minimum to another via an intermediate maximum. The Transition state is the configuration which divides the reactant and product parts of surface. For example, a molecule which has reached the transition state will continue on to product. The geometrical configuration of the energy maximum is called the transition–state structure. Within standard TST, the transition state and transition–state structure are identical, but this is not necessarily for more refined models. The direction of reaction coordinate is started from the reactant to product along a path where the energies are as low as possible and the TS is the point where the energy has a maximum, shown in Figure 2.1.
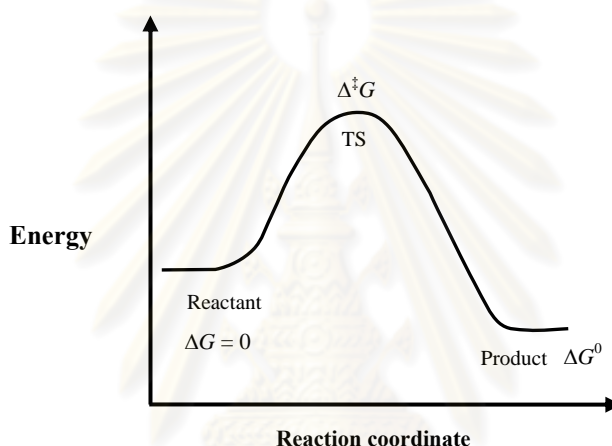
Figure 2.1 Schematic illustration of reaction path.

2.4.1 Rate constant and Boltzman distribution

TST assumes equilibrium energy distribution among all possible quantum states at all points along the reaction coordinates. The probability of finding a molecule in a given quantum state is proportional to $e^{-\Delta E/k_B T}$, which is Boltzman distribution. Assuming that the molecule at the TS is in equilibrium with the reactant, the macroscopic rate constant can be expressed as

$$k = \frac{k_B T}{hc^0} e^{-\Delta^{\ddagger} G/RT} \tag{2.26}$$

$\Delta^{\ddagger}G$ is the Gibbs free energy difference between the TS and reactant, T is absolute temperature and k_B is Boltzmann's constant and c^0 is concentration factor. From the

TST expression (2.26) it is clear that if the free energy of the reactant and TS can be calculated, the reaction rate follows trivially. The equilibrium constant for a reaction can be calculated from the free energy difference between the reactant(s) and product(s).

$$K_{eq} = e^{-\Delta G_0 / RT} \tag{2.27}$$

The Gibbs free energy is given in terms of the enthalpy and entropy, $G = H - TS$.

2.4.2 Rate constant with tunneling corrections

Tunneling corrections were calculated using the Wigner, Eckart [26], the multi–dimensional zero–curvature (ZCT) [27] and centrifugal–dominant small–curvature (SCT) [28] methods. The Wigner method is a simple, zeroth–order tunneling approximation and only depends on the curvature at transition state. The Eckart method is believed to be one of the more accurate approximate one dimensional tunneling corrections. The Eckart tunneling factor is calculated by fitting an Eckart potential to the MEP using the curvature at the transition state, the zero–point energy inclusive energy barrier, and the reaction energy. The ZCT method is a minimum–energy–path, semiclassical adiabatic ground–state (MEPSAG) method which takes into account tunneling along the MEP. Reaction path curvature and coupling to modes orthogonal to the MEP are neglected. The SCT method is a centrifugal–dominant small–curvature semi–classical adiabatic ground–state (CD–SCSAG) method which accounts for the curvature of the reaction path and approximately incorporates tunneling paths other than the MEP.
Reaction rate coefficients were calculated using the

$$k = \kappa \left[\frac{k_B T}{h} \right] \left[\frac{Q_{TS}}{Q_{Complex}} \right] e^{-\Delta^{\ddagger} E / RT} \tag{2.28}$$

where tunneling factor, $\kappa = 1 + (1/24)(h v_i c / k_B T)^2$, k_B is Boltzman constant, T is absolute temperature, Q_{TS} and $Q_{Complex}$ are the partition functions of transition state

and complex, respectively, h is Plank constant, c is speed of light and v_i is imaginary frequency of transition state.

2.4.3 Partition functions

The first step in determining the thermal contributions to the enthalpies and entropies of a molecule is to determine its partition function, q which is a measure of the number of accessible to the molecule (translational, rotational, vibrational and electronic states) at a particular temperature.

It is assumed that the translational (T), rotational (R), vibrational (V) and electronic (E) modes of the system can be separated, thus allowing the energy of each level, E_i, to be separated into T, R, V and E contributions as

$$E = E_i^T + E_i^R + E_i^V + E_i^E \tag{2.29}$$

While the translational modes are truly independent from the rest, the separations of other modes are based on an approximation, in particular the Bohn–Oppenheimer approximation for electronic and vibrational motion and the rigid rotor approximation which assumes (that the geometry of the molecule does not change as it rotates) for vibrational and rotational modes. Within these approximations, the total molecular partition function can therefore be factorized into translational, rotational, vibrational and electronic contributions:

$$q = q_{trans} q_{vib} q_{rot} q_{elect} \tag{2.30}$$

2.4.3.1 Translational partition function

For bimolecular reactions, the ratio of the translational partition functions may be simplified to yield the relative translational partition in per unit volume as

$$q_{trans} = \frac{V}{\Lambda^3} \tag{2.31}$$

$$\Lambda = h\left(\frac{\beta}{2\pi m}\right)^{1/2} \tag{2.32}$$

where h is Planck's constants, m is the mass of the molecule and V is the available volume to it. For a gas phase system this is the molar volume (usually determined by the ideal gas equation) at the specific temperature and pressure.

2.4.3.2 Vibrational partition function

The vibrational partition functions are calculated quantum mechanically within the framework of the harmonic approximation. The harmonic oscillator partition function is given by:

$$q_{trans} = \prod_i \frac{1}{1 - e^{-\beta hc\tilde{v}}}$$

(2.33)

where $\tilde{v}_i$ is the vibrational frequency in cm^{-1} for mode i. The product is over all vibrational modes.

2.4.3.3 Rotational partition function

The formulation for rotational partition functions depends on whether or not the molecule is linear. For linear molecules

$$q_{rot} = \frac{k_B T}{\sigma hcB}$$

(2.34)

and for non linear

$$q_{rot} = \frac{1}{\sigma} \left(\frac{k_B T}{hc} \right)^{3/2} \left(\frac{\pi}{ABC} \right)^{1/2}$$

(2.35)

where σ is the rotational symmetry number of the molecule, c is the speed of light and A, B, C are the rotational constants.

2.4.3.4 Electronic partition function

For the electronic partition function, an adiabatic potential energy surface is assumed. The electronic degeneracies along the MEP are assumed to be the same as at the transition state. The formula employed is

$$q_{elect} = \omega_{e1} + \omega_{e1} \exp(-\beta \Delta \varepsilon_{12}) + ... \tag{2.36}$$

where $\Delta \varepsilon_{1j}$ is the energy of the jth electronic level relative to the ground state and ω_{ej} is the corresponding degeneracy.

2.5 Molecular vibrational frequencies

The total molecular energy E is approximately the sum of translation, rotational, vibrational, and electronic energies. In the harmonic oscillator approximation, the vibrational energy of an N–atom molecule is the sum of 3N–6 normal mode vibrational energies (3N–5 for a linear molecule) [29]:

$$E_{vib} \approx \sum_{k=1}^{3N-6} (\upsilon_k + \frac{1}{2}) h v_k \tag{2.37}$$

where v_k is the harmonic vibrational frequency for the kth normal mode and each vibrational quantum number υ_k has the possible values 0, 1, 2,..., independent of the value of the order vibrational quantum numbers.

The harmonic vibrational frequencies of a molecule are calculated as follows. (1) Solve the electronic Schrödinger equation $(\hat{H}_{el} + V_{NN})\psi_{el} = U\psi_{el}$ for several molecular geometries to find the equilibrium geometry of the molecule. (2) Calculate the set of second derivatives $(\partial^2 U / \partial X_i \partial X_j)_e$ of the molecular electronic energy U with respect to the 3N nuclear Cartesian coordinates of a coordinate system with origin at the center of mass. (3) Form the mass–weighted force–constant matrix elements

$$F_{ij} = \frac{1}{(m_i m_j)^{1/2}} \left(\frac{\partial^2 U}{\partial X_i \partial X_j} \right)_e \qquad (2.38)$$

where i and j each go from 1 to 3N and m_i is the mass of the atom corresponding to coordinate X_i. (4) Solve the following set of 3N linear equations in 3N unknowns

$$\sum_{j=1}^{3N} (F_{ij} - \delta_{ij} \lambda_k) l_{jk} = 0 \qquad i = 1, 2,..., 3N \qquad (2.39)$$

In this set of equations, δ_{ij} is the Kronecker delta, and λ_k and the l_{jk}'s are as–yet unknown parameters whose significance will be seen shortly. In order that this set of homogeneous equations has a nontrivial solution, the coefficient determinant must vanish

$$\det(F_{ij} - \delta_{ij} \lambda_k) = 0 \qquad (2.40)$$

This determinant is of order 3N and when expanded gives a polynomial whose highest power of λ_k is λ_k^{3N}. The molecular harmonic vibrational frequencies are then calculated from

$$v_k = \lambda_k^{1/2} / 2\pi \qquad (2.41)$$

Six of the λ_k values found by solving will be zero, yielding six frequencies with value zero, corresponding to the three translational and three rotational degrees of freedom of the molecule. The remaining 3N–6 vibrational frequencies are the molecular harmonic vibrational frequencies.

2.6 Thermochemistry

The usual way to calculate enthalpies of reaction is to calculate heats of formation, and take the appropriate sums and difference [30].

$$\Delta_r H^{\circ}(298\,K) = \sum_{products} \Delta_f H^{\circ}_{prod}(298\,K) - \sum_{reactants} \Delta_f H^{\circ}_{react}(298\,K) \qquad (2.42)$$

However, since Gaussian provides the sum of electronic and thermal enthalpies, there is a short cut: namely, to simply take the difference of the sums of these values for the reactants and the products.

Calculating enthalpies of formation is a straight–forward, albeit somewhat tedious task, which can be split into a couple of steps. The first step is to calculate the enthalpies of formation $(\Delta_f H^{o}(0K))$ of the species involved in the reaction. The second step is to calculate the enthalpies of formation of the species at 298 K. Calculating the Gibbs free energy of reaction is similar, except we have to add in the entropy term:

$$\Delta_f G^{\circ}(298\,K) = \Delta_f H^{\circ}(298\,K) - T(S^{\circ}(M, 298\,K) - \sum S^{\circ}(X, 298\,K)) \qquad (2.43)$$

To calculate these quantities, we need a few component pieces first. In the descriptions below, I will use M to stand for the molecule, and X to represent each element which makes up M, and x will be the number of atoms of X in M.

- Atomization energy of the molecule, $\sum D_0(M)$:

  These are readily calculated from the total energies of the molecule $\sum \varepsilon_0(M)$, the zero–point energy of the molecule $(\varepsilon_{ZPE}(M))$ and the constituent atoms:

$$\sum D_0(M) = \sum_{atoms} x\varepsilon_0(X) - \varepsilon_0(M) - \varepsilon_{ZPE}(M) \qquad (2.44)$$

- Heats of formation of the atoms at 0K, $(\Delta_f H^{\circ}(X, 0K))$ [31]

- Enthalpy corrections of the atomic elements, $H^{\circ}_x(298\,K) - H^{\circ}_x(0K)$

- Enthalpy correction for the molecule, $H_M^{\circ}(298K) - H_M^{\circ}(0K)$

- Entropy for the atoms, $S_x^{\circ}(298K)$

- Entropy for the molecule, $S_M^{\circ}(298K)$

Putting all these pieces together, we can finally take the steps necessary to calculate $\Delta_f H^{\circ}(298K)$ and $\Delta_f G^{\circ}(298K)$:

1. Calculate $\Delta_f H^{\circ}(M, 0K)$ for each molecule:

$$\Delta_f H^{\circ}(M, 0K) = \sum_{atoms} x\Delta_f H^{\circ}(X, 0K) - \sum D_0(M)$$
$$= \sum_{atoms} x\Delta_f H^{\circ}(X, 0K) - (\sum_{atoms} x\varepsilon_0(X) - \varepsilon_0(M)) \quad (2.45)$$

2. Calculate $\Delta_f H^{\circ}(M, 298K)$ for each molecule:

$$\Delta_f H^{\circ}(M, 298K) = \Delta H_f^{\circ}(M, 0K) + (H_M^{\circ}(298K) - H_M^{\circ}(0K))$$
$$- \sum_{atoms} x(H_X^{\circ}(298K) - H_X^{\circ}(0K)) \quad (2.46)$$

3. Calculate $\Delta_f G^{\circ}(M, 298K)$ for each molecule:

$$\Delta_f G^{\circ}(M, 298K) = \Delta_r H^{\circ}(298K) + 298.15(S^{\circ}(M, 298K) - \sum S^{\circ}(X, 298K)) \quad (2.47)$$

CHAPTER III

DETAILS OF THE CALCULATIONS

3.1 Computational method

The optimized structures for all related compounds in olefination reaction, their corresponding transition states and configurations of their interactions were carried out using density functional theory (DFT) method. The calculations were performed by hybrid density functional B3LYP, the Becke's three–parameter exchange functional [32] with the Lee–Yang–Parr correlation functional [33], using the Los Alamos National Laboratory (LanL)'s small effective core potentials with double zeta valence basis set (DZ), namely, LanL2DZ [34–36]. The zero point vibrational energy (ZPVE) corrections were obtained from frequency calculations at the B3LYP/LanL2DZ level of theory. The transition–state structures obtained at the B3LYP/LanL2DZ level have been located using the reaction coordinate method referred to the synchronous transit–guided quasi–newton (STQN) calculation [37]. The intrinsic reaction coordinate (IRC) method [38] was used to track minimum energy paths from transition structures to the corresponding minimum. All the transition states were confirmed by single imaginary vibrational frequency. The optimized structures for all the complexes with copper oxide–pillared clay (Cu–pillared clay) catalyst have been carried out at the UB3LYP/LanL2DZ level of the doublet spin state except the Cu–pillared clay catalyst complexes interacting with CCl_4 namely the species of **TS6_A, 13A, TS7_A, 14A, 15A, TS6_B, 13B, TS7_B, 14B, 15B, TS6_C, 13C, TS7_C, 14C, 15C, TS6_D, 13D, TS7_D, 14D, 15D, TS6_E, 13E, TS7_E, 14E, 15E, 17, TS8** and **18,** the quartet spin state being used. The spin states and spin contaminations for all related species are listed in Table A-1 to A-6 in appendix A. The solvent effect was investigated by single–point computations on the LanL2DZ–optimized gas–phase structures using the conductor–like polarizable continuum model (CPCM) [39] which is based on the polarized continuum model (PCM) of Tomasi and co–workers [40–45]. All calculations were performed using GAUSSIAN 03 program [46].

The standard enthalpy ΔH°_{298} and Gibbs free energy change ΔG°_{298} of reactions have been derived from the ZPVE [47] computed at the same level of theory which has been employed for structure optimizations. The rate constants $k(T)$ for conversion reactions have been derived from the transition state theory with and without tunneling effects, respectively. The rate constants for each reaction steps of olefination in DMSO and in gas phase were computed using Eq. (2.26) and Eq. (2.28), respectively.

CHAPTER IV

RESULTS AND DISCUSSION

In the present study, reaction mechanisms of olefination of halogenobenzaldehyde compounds with hydrazine and carbontetrachloride (CCl_4) to form dihalogenovinyl halogenobenzene compounds have been studied using copper oxide–pillared clay (Cu–pillared clay) as a catalyst. The halogenobenzaldehyde reactants studied in this work are 4–chlorobenzaldehyde (4CBD), 3–chlorobenzaldehyde (3CBD), 4–bromobenzaldehyde (4BBD), 3–bromobenzaldehyde (3BBD) and benzaldehyde (BD) and their corresponding products are 1–(2,2–dichlorovinyl)–4–chlorobenzene (DCV4CB), 1–(2,2–dichlorovinyl)–3–chlorobenzene (DCV3CB), 1–(2,2–dichlorovinyl)–4–bromobenzene (DCV4BB), 1–(2,2–dichlorovinyl)–3–bromobenzene (DCV3BB) and 1–(2,2–dichlorovinyl)–benzene (DCVB), respectively. Reaction mechanisms of conversions of 4CBD to DCV4CB, 3CBD to DCV3CB, 4BBD to DCV4BB, 3BBD to DCV3BB and BD to DCVB were investigated and their reaction energies, rate constant and equilibrium constant were obtained. The optimized structures for all related compounds in olefination for syntheses of alkene compounds, their corresponding transition states and configurations of their interactions were obtained using the B3LYP/LanL2DZ method. The structure optimizations for all the complexes with Cu–pillared clay catalyst have been carried out at the UB3LYP/LanL2DZ method with the doublet spin state except the species of Cu–pillared clay complexes interacting with CCl_4, the quartet spin state being used. The spin states and spin contaminations for all studied species are listed in Tables A-1 to A-6 in, in Appendix A.

4.1 Reaction mechanism of olefination of 4CBD to DCV4CB product

The B3LYP/LanL2DZ optimized structures of compounds involved in the first three reaction processes and potential energy profiles for the reaction of 4CBD and hydrazine to form DCV4CB product are shown in Figures 4.1–4.3; their transition–state structures are shown in Figures 4.4–4.6 and their imaginary frequencies are shown in Table 4.1.
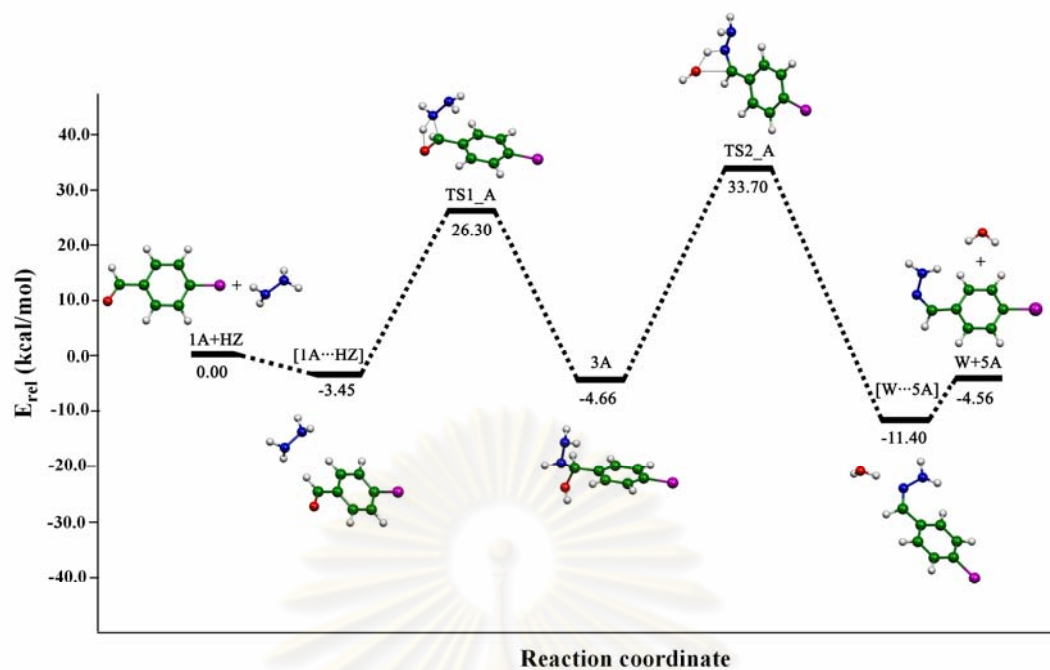
Figure 4.1 Potential energy profile for precursor formation of 4CBD and hydrazine to form hydrazone.
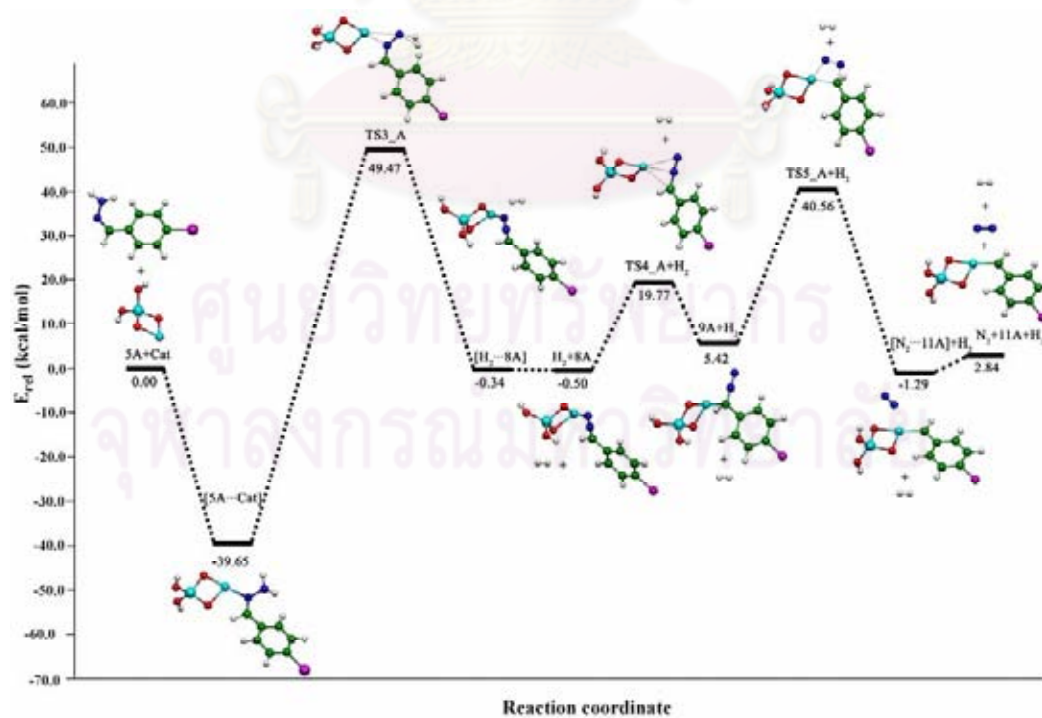
Figure 4.2 Potential energy profile for dehydrogenation and denitrogenation to form olefinic intermediate in 4CBD reactant system.
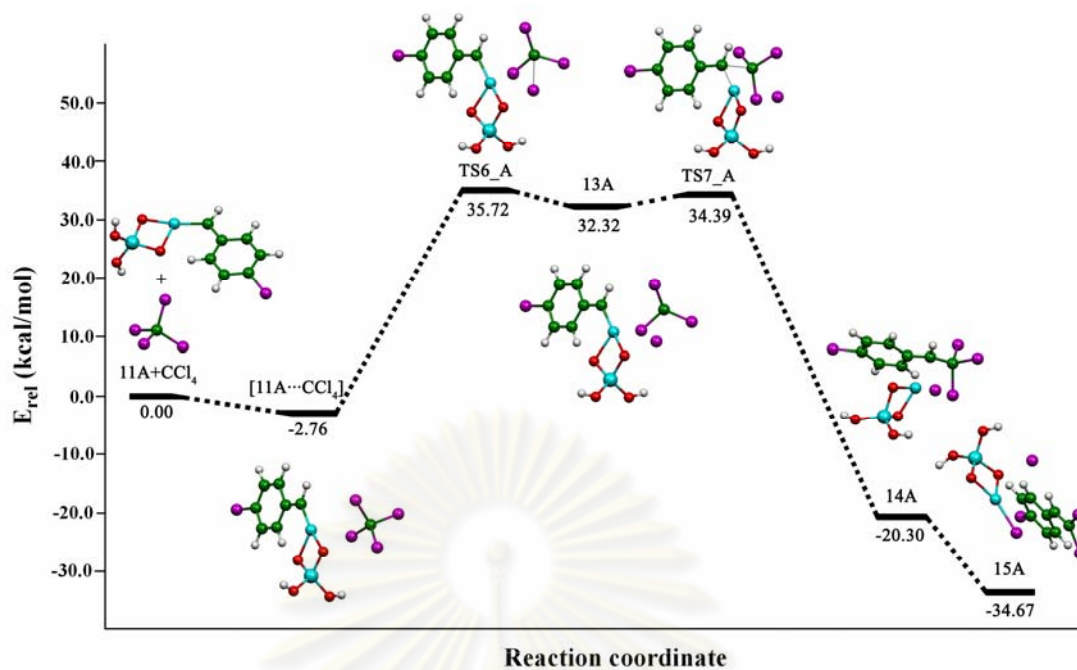
Figure 4.3 Potential energy profile for the chlorination of olefinic intermediate with CCl$_4$ to form the complex of DCV4CB product and the dichloro Cu–pillared clay catalyst.
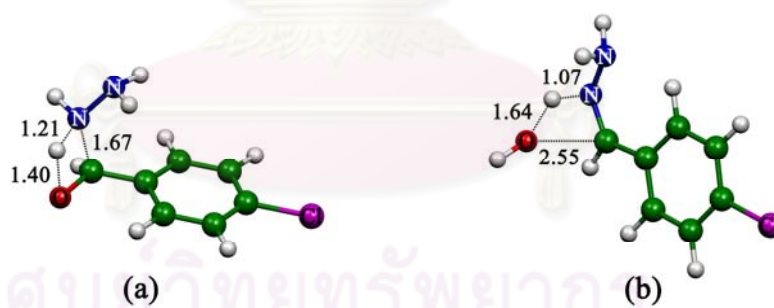
Figure 4.4 The B3LYP/LanL2DZ–optimized transition–state structures for precursor formation of 4CBD and hydrazine to form hydrazone (a) TS1_A and (b) TS2_A. Bond distances are in Å.
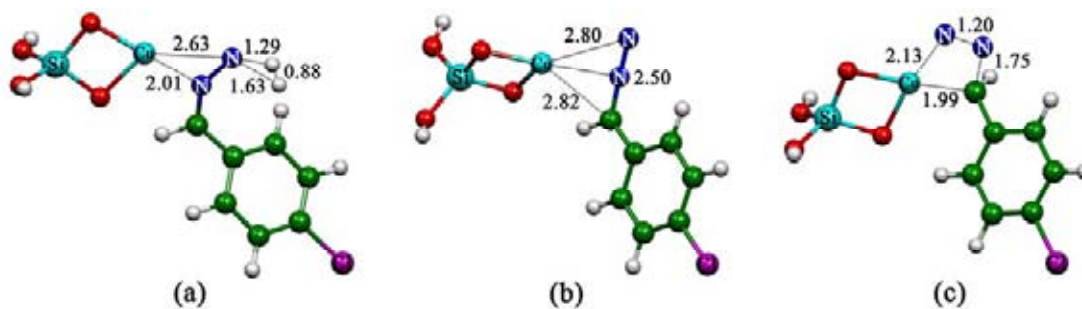
Figure 4.5 The B3LYP/LanL2DZ–optimized transition–state structures for dehydrogenation and denitrogenation to form olefinic intermediate in 4CBD reactant system (a) TS3_A, (b) TS4_A and (c) TS5_A. Bond distances are in Å.
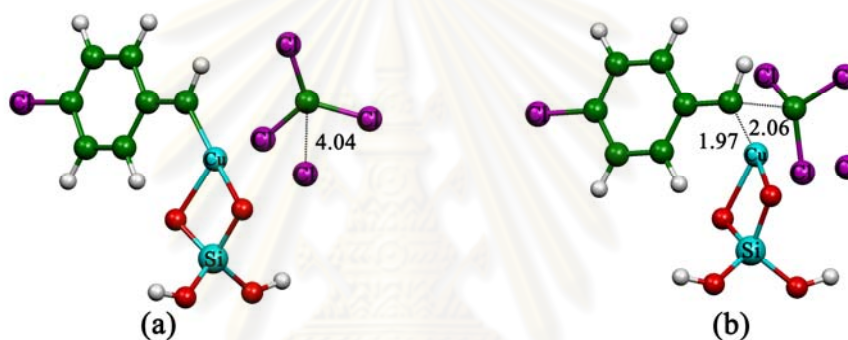
Figure 4.6 The B3LYP/LanL2DZ–optimized transition–state structures for chlorination of olefinic intermediate with CCl_4 to form the complex of DCV4CB product and dichloro Cu–pillared clay catalyst (a) TS6_A and (b) TS7_A. Bond distances are in Å.

Table 4.1 Imaginary frequencies for transition states of the DCV4CB product

transition state	imaginary frequency, cm^{-1}
TS1_A	–1429.28
TS2_A	–475.36
TS3_A	–1238.55
TS4_A	–134.19
TS5_A	–337.45
TS6_A	–334.69
TS7_A	–86.14

Potential energy profile for precursor formation of 4CBD and hydrazine (**HZ**) to form hydrazone is shown in Figure 4.1. The precursor process is composed of four reaction steps, **1A** + **HZ** → [**1A···HZ**], [**1A···HZ**] → **TS1_A**→ **3A**, **3A** → **TS2_A** → [**W···5A**] and [**W···5A**] → **W** (water) + **5A** as shown in Figure 4.1. The last step of the precursor process is dehydration reaction. Compounds **1A** and **HZ** represent the 4CBD reactant and hydrazine, respectively. The precursor process is association of **1A** and **HZ** affording **3A** and dehydration reaction of **3A** to afford an intermediate precursor (**5A**) which is a hydrazone.

Figure 4.2 shows the potential energy profile for the dehydrogenation and denitrogenation to form olefinic intermediate, computed at the B3LYP/LanL2DZ levels of theory. It shows the potential energy profile for the dehydrodenitrogenation comprises six reaction steps, **5A** + **Cat** → [**5A···Cat**], [**5A···Cat**] → **TS3_A** → [**H$_2$···8A**], [**H$_2$···8A**] → **H$_2$** + **8A**, **8A** → **TS4_A** → **9A**, **9A** → **TS5_A** → [**N$_2$···11A**] and [**N$_2$···11A**] → **N$_2$** + **11A.** The [**5A···Cat**] → **TS3_A** → [**H$_2$···8A**] was found to be the rate–determining step. The **5A** precursor associates with the Cu–pillared clay catalyst (**Cat**) to form [**5A···Cat**] intermediate and it dehydrogenated to afford compound **8A**. Compound **8A** rearranged via transition state **TS4_A** to afford **9A**. The denitrogenation of **9A** occurs via transition state **TS5_A** to afford **11A** which is the p–chlorophenylmethyl complex with Cu–pillared clay catalyst as a copper–carbene complex.

The chlorination of olefinic intermediate with CCl$_4$ to form the complex of DCV4CB product and the dichloro Cu–pillared clay catalyst is shown in Figure 4.3. This chlorination process is composed of four reaction steps namely **11A** + **CCl$_4$** → [**11A···CCl$_4$**], [**11A···CCl$_4$**] → **TS6_A** → **13A**, **13A** → **TS7_A** → **14A** and **14A** → **15A**. The first step is an association of compound **11A** with **CCl$_4$** to form [**11A···CCl$_4$**] and afford intermediate **13A** via transition state **TS6_A**. The association complex of chlorinated intermediate and Cu–pillared clay catalyst (**14A**) is obtained via transition state **TS7_A**, and rearranged to form compound **15A**.

Relative energies of all related species for synthesis of the DCV4CB product in gas phase and in DMSO are listed in Table 4.2. It shows that the relative energies of all related species for synthsis of the DCV4CB product in gas phase are similar to the energies in DMSO. Reaction energies, thermodynamic properties, rate and equilibrium constants for synthetic reaction of DCV4CB product in gas phase and in DMSO are shown in Table 4.3 and Table 4.4, respectively. The rate constants in

DMSO were computed using Eq. (2.26) whose formulae is a function of the free energy at activation of solvation state ($\Delta\Delta^{\ddagger}G$) are shown in Table 4.4. The Gibbs free energies at activations of the rate–determining step in gas phase is smaller than in DMSO by 20.3 kcal/mol this indicates that the reaction in gas phase is more preferable process rather than in DMSO.

Table 4.2 Relative energies (in kcal/mol) of all related species for synthesis of the DCV4CB product in gas phase and in DMSO, computed at the B3LYP/LanL2DZ

Reactions/Species	ΔE_{rel}	
	In gas phase	In DMSO
Precursor formation: [a]		
1A + HZ	0.00	0.00
[1A⋯ HZ]	−3.45	−2.59
TS1_A	26.30	24.13
3A	−4.66	−3.59
TS2_A	33.70	35.82
[W⋯5A]	−11.40	−9.16
W + 5A	−4.56	−5.93
Dehydrodenitrogenatio: [b]		
5A + Cat	0.00	0.00
[5A⋯Cat]	−39.65	−37.18
TS3_A	49.47	54.87
[H_2⋯8A]	−0.34	6.33
H_2 + 8A	−0.50	4.11
TS4_A + H_2	19.77	27.01
9A + H_2	5.42	8.87
TS5_A + H_2	40.56	46.89
[N_2⋯11A] + H_2	−1.29	5.66
N_2 + 11A + H_2	2.84	3.90
Chlorination: [c]		
11A + CCl_4	0.00	0.00
[11A⋯CCl_4]	−2.76	3.37
TS6_A	35.72	41.71
13A	32.32	38.20
TS7_A	34.39	40.68
14A	−20.30	−6.41
15A	−34.67	−27.10

[a] Relative to the sum of total energies of 1 and 2.

[b] Relative to the sum of total energies of 5 and 6.

[c] Relative to the sum of total energies of 11 and 12.

Table 4.3 Reaction energies, thermodynamic properties, rate and equilibrium constants for synthetic reaction of DCV4CB product in gas phase

| Reaction	$\Delta^{\ddagger}E$ [a,b]	$\Delta^{\ddagger}G$ [a,b]	k_{298} [c]	ΔE [a]	ΔH_{298} [a]	ΔG_{298} [a]	K_{298}
Precursor formation:							
1A + HZ → [1A···HZ]	–	–	–	– 3.45	– 3.02	4.72	3.48×10^{-4}
[1A···HZ] →TS1_A → 3A	29.75	38.37	1.56×10^{-11}	– 1.21	– 2.39	1.66	6.04×10^{-2}
3A → TS2_A → [W···5A]	38.36	38.37	6.05×10^{-16}	– 6.74	– 5.77	– 9.10	4.65×10^{6}
[W···5A] → W + 5A	–	–	–	6.84	7.12	– 0.32	1.70×10^{0}
Dehydrodenitrogenation:							
5A + Cat[d] → [5A···Cat]	–	–	–	– 39.65	– 38.93	– 28.20	4.71×10^{20}
[5A···Cat] → TS3_A → [H₂···8A]	89.12	88.48	2.09×10^{-52}	39.31	41.20	33.39	3.32×10^{-25}
[H₂···8A] → H₂ + 8A	–	–	–	– 0.16	0.07	– 4.26	1.33×10^{3}
8A → TS4_A → 9A	20.28	21.65	7.21×10^{-4}	5.92	5.80	8.36	7.43×10^{-7}
9A → TS5_A → [N₂···11A]	35.14	35.95	2.97×10^{-14}	– 6.70	– 5.74	– 8.63	2.10×10^{6}
[N₂···11A] → N₂ + 11A	–	–	–	4.13	3.75	– 2.95	1.45×10^{2}
Chlorination :							
11A + CCl₄ → [11A···CCl₄]	–	–	–	– 2.76	– 1.82	4.41	5.85×10^{-4}
[11A···CCl₄] → TS6_A → 13A	38.48	36.13	3.39×10^{-14}	35.08	35.58	33.41	3.21×10^{-25}
13A → TS7_A → 14A	2.08	6.32	1.18×10^{8}	– 52.62	– 53.22	– 49.06	9.18×10^{35}
14A → 15A[e]	–	–	–	– 14.36	– 14.30	– 14.49	4.19×10^{10}

[a] In kcal/mol.

[b] Activation state.

[c] Computed using Eq. 2.28, in s^{-1}.

[d] Cu–pillared clay catalyst.

[e] The complex of 1–(2,2–dichlorovinyl)–4–chlorobenzene (DVC4CB) with the dichloro Cu–pillared clay catalyst.

Table 4.4 Reaction energies, Gibbs free energies, rate and equilibrium constants for synthetic reaction of the DCV4CB product in DMSO

Reaction	$\Delta\Delta^{\ddagger}G$ [a,b,c]	k_{298} [d]	$\Delta\Delta G_{298}$ [a,c]	K_{298}
Precursor formation:				
1A + HZ → [1A··· HZ]	–	–	–0.91	4.61×10^{0}
[1A··· HZ] →TS1_A → 3A	26.63	1.88×10^{-7}	–4.21	1.22×10^{3}
3A → TS2_A → [W···5A]	41.71	1.66×10^{-18}	–4.47	1.89×10^{3}
[W···5A] → W + 5A	–	–	5.58	8.13×10^{-5}
Dehydrodenitrogenation:				
5A + Cat[e] → [5A···Cat]	–	–	–38.77	2.62×10^{28}
[5A···Cat] → TS3_A → [H₂···8A]	101.94	1.16×10^{-62}	53.72	4.16×10^{-40}
[H₂···8A] → H₂ + 8A	–	–	0.31	5.91×10^{-1}
8A → TS4_A → 9A	24.74	4.57×10^{-6}	5.69	6.75×10^{-5}
9A → TS5_A → [N₂···11A]	40.61	1.06×10^{-17}	–2.18	3.98×10^{1}
[N₂···11A] → N₂ + 11A	–	–	2.85	8.17×10^{-3}
Chlorination :				
11A + CCl₄ → [11A···CCl₄]	–	–	0.81	2.55×10^{-1}
[11A···CCl₄] → TS6_A → 13A	44.35	1.91×10^{-20}	40.52	1.98×10^{-30}
13A → TS7_A → 14A	0.33	3.57×10^{12}	–48.65	4.60×10^{35}
14A → 15A[f]	–	–	–20.87	1.98×10^{15}

[a] In kcal/mol.

[b] Activation state.

[c] In DMSO, derived from the single–point CPCM calculation (ε=46.7) at the B3LYP/LanL2DZ level.

[d] Computed using Eq. (2.26), in s^{-1}.

[e] Cu–pillared clay catalyst.

[f] The complex of 1–(2,2–dichlorovinyl)–4–chlorobenzene with the di–chlorinated Cu–pillared clay catalyst.

Table 4.3 shows that free energies of reaction steps, **3A → TS2_A → [W···5A]**, **[W···5A] → W + 5A**, **5A + Cat → [5A···Cat]**, **[H₂···8A] → H₂ + 8A**, **9A → TS5_A → [N₂···11A]**, **[N₂···11A] → N₂ + 11A**, **13A → TS7_A → 14A** and **14A → 15A** are spontaneous reactions but the other reaction are non–spontaneous. The reaction steps, **1A + HZ → [1A···HZ]**, **[1A···HZ] → TS1_A → 3A**, **3A → TS2_A → [W···5A]**, **5A + Cat → [5A···Cat]**, **9A → TS5_A → [N₂···11A]**, **11A + CCl₄ → [11A···CCl₄]**, **13A → TS7_A → 14A** and **14A → 15A** are found to be an exothermic reaction. The magnitudes of rate constants of all reaction steps are in order: **13A → TS7_A → 14A** (1.18×10^{8} s^{-1}) > **8A → TS4_A → 9A** (7.21×10^{-4} s^{-1}) > **[1A···HZ] → TS1_A → 3A** (1.56×10^{-11} s^{-1}) > **9A → TS5_A → [N₂···11A]** (2.97×10^{-14} s^{-1}) > **[11A···CCl₄] → TS6_A → 13A** (3.39×10^{-14} s^{-1}) > **3A → TS2_A → [W···5A]** (6.05×10^{-16} s^{-1}) > **[5A···Cat] → TS3_A → [H₂···8A]** (2.09×10^{-52} s^{-1}).

Reaction energies, Gibbs free energies, rate and equilibrium constants of all reaction steps in DMSO compound using solvent effect calculation at the B3LYP/LanL2DZ level, shown in Table 4.4 are in agreement with the values in gas phase. Magnitude of all their rate constants in gas phase and DMSO are in the same order.

Activation energies, tunneling coefficients, A factors and rate constants for synthetic reaction of DCV4CB product are shown in Table 4.5. The rate constants were computed using Eq. (2.28) of which formulae also depends on the magnitude of imaginary frequency of the corresponding transition state. The pre–exponential parameters (κ.A) are acceptable values as compare with any exponential results.

Table 4.5 Activation energies, tunneling coefficients, A factors and rate constants for synthetic reaction of DCV4CB product, computed at the B3LYP/LanL2DZ in gas phase

Reaction	κ^a	Q_{TS}/Q_{REA}	A^b	$\Delta^{\ddagger}E^c$	$k_{298}{}^d$
Precursor formation:					
$1A + HZ \rightarrow [1A\cdots HZ]$	–	–	–	–	–
$[1A\cdots HZ] \rightarrow TS1\_A \rightarrow 3A$	2.98	5.44×10^{-3}	3.38×10^{10}	29.75	1.56×10^{-11}
$3A \rightarrow TS2\_A \rightarrow [W\cdots 5A]$	1.22	1.06×10^{0}	6.59×10^{12}	38.36	6.05×10^{-16}
$[W\cdots 5A] \rightarrow W + 5A$	–	–	–	–	–
Dehydrodenitrogenation:					
$5A + Cat^e \rightarrow [5A\cdots Cat]$	–	–	–	–	–
$[5A\cdots Cat] \rightarrow TS3\_A \rightarrow [H_2\cdots 8A]$	2.49	2.92×10^{0}	1.82×10^{13}	89.12	2.09×10^{-52}
$[H_2\cdots 8A] \rightarrow H_2 + 8A$	–	–	–	–	–
$8A \rightarrow TS4\_A \rightarrow 9A$	1.02	8.36×10^{-2}	5.19×10^{11}	20.28	7.21×10^{-4}
$9A \rightarrow TS5\_A \rightarrow [N_2\cdots 11A]$	1.11	2.49×10^{-1}	1.55×10^{12}	35.14	2.97×10^{-14}
$[N_2\cdots 11A] \rightarrow N_2 + 11A$	–	–	–	–	–
Chlorination :					
$11A + CCl_4 \rightarrow [11A\cdots CCl_4]$	–	–	–	–	–
$[11A\cdots CCl_4] \rightarrow TS6\_A \rightarrow 13A$	1.11	8.03×10^{1}	4.99×10^{14}	38.48	3.39×10^{-14}
$13A \rightarrow TS7\_A \rightarrow 14A$	1.01	6.27×10^{-4}	3.90×10^{9}	2.08	1.18×10^{8}
$14A \rightarrow 15A^f$	–	–	–	–	–

[a] $\kappa = 1 + \dfrac{1}{24}\left(\dfrac{h\nu_i}{k_B T}\right)^2$.

[b] $A = \dfrac{k_B T}{h}\dfrac{Q_{TS}}{Q_{REA}}$, in s^{-1}.

[c] Computed with ZPVE corrections, in kcal/mol.

[d] Computed using Eq. 2.28, in s^{-1}.

[e] Cu–pillared clay catalyst.

[f] The complex of 1–(2,2–dichlorovinyl)–4–chlorobenzene (DCV4CB) with the dichloro Cu–pillared clay catalyst.

**4.2 Reaction mechanism of olefination of 3CBD to DCV3CB product**

   The potential energy profiles for the reaction of 3CBD and hydrazine to form DCV3CB product are shown in Figures 4.7–4.9; their transition–state structures are shown in Figures 4.10–4.12 and their imaginary frequencies are shown in Table 4.6. Reaction energies, thermodynamic properties, rate and equilibrium constants for synthetic reaction of DCV3CB product in gas phase are shown in Table 4.7.
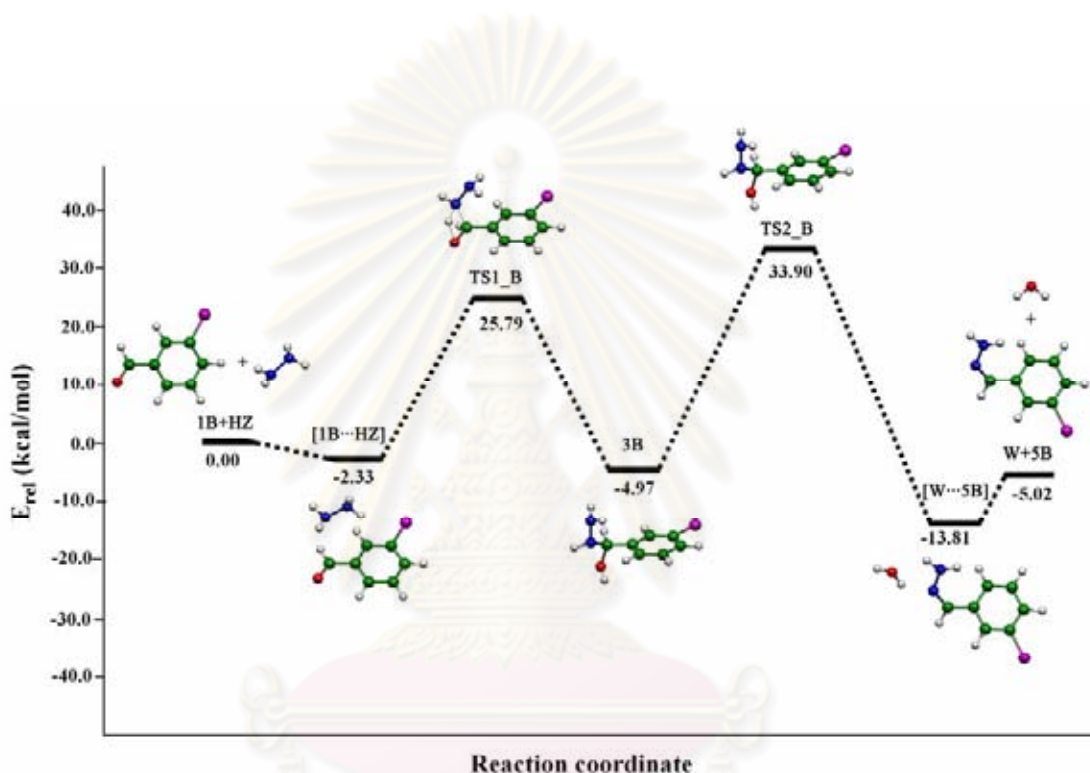
Figure 4.7 Potential energy profile for precursor formation of 3CBD and hydrazine to form hydrazone.
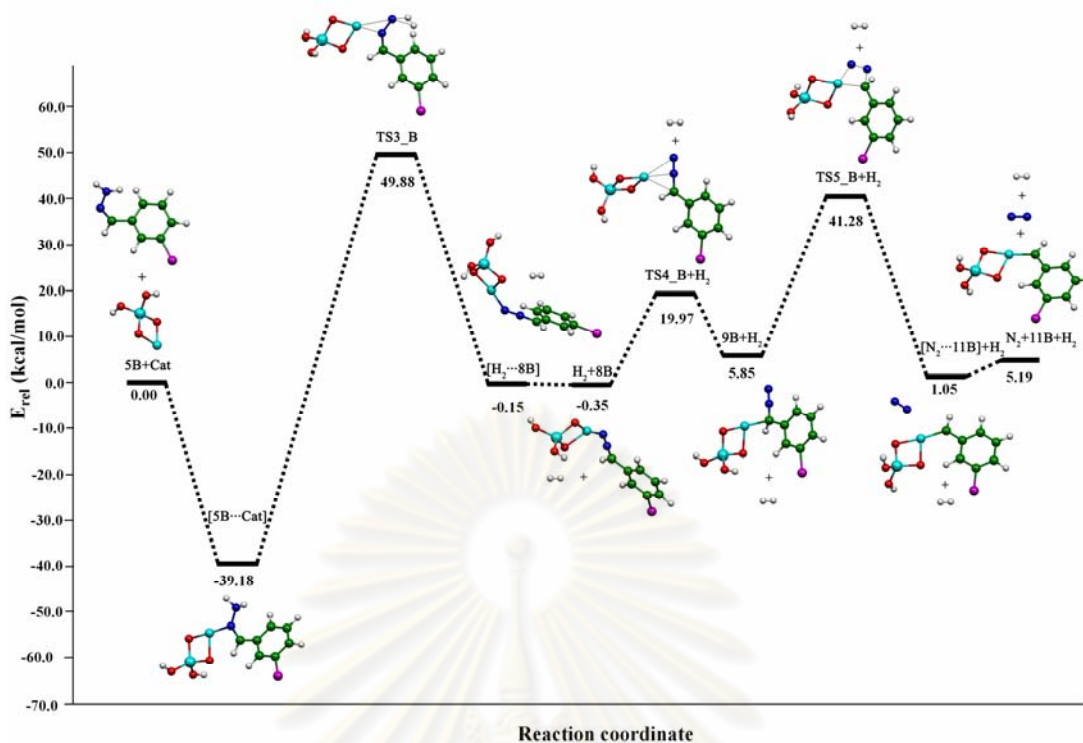
Figure 4.8 Potential energy profile for dehydrogenation and denitrogenation to form olefinic intermediate in 3CBD reactant system.
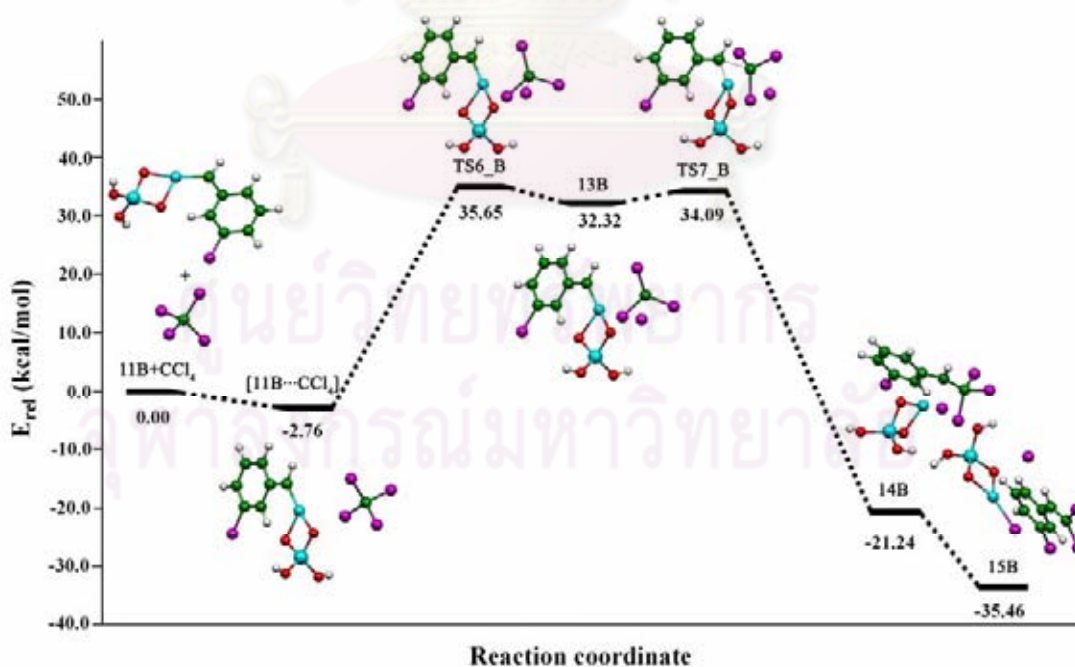
Figure 4.9 Potential energy profile for the chlorination of olefinic intermediate with CCl_4 to form the complex of DCV3CB product and the dichloro Cu–pillared clay catalyst.
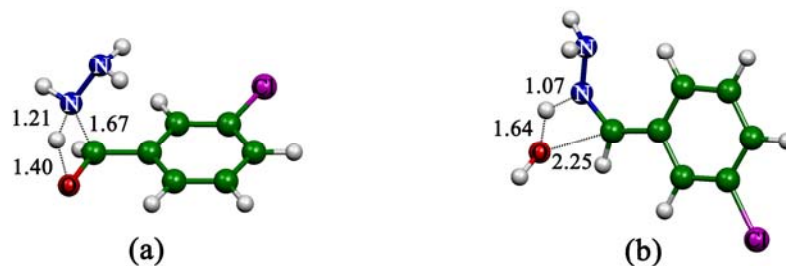
Figure 4.10 The B3LYP/LanL2DZ–optimized transition–state structures for precursor formation of 3CBD and hydrazine to form hydrazone (a) TS1_B and (b) TS2_B. Bond distances are in Å.
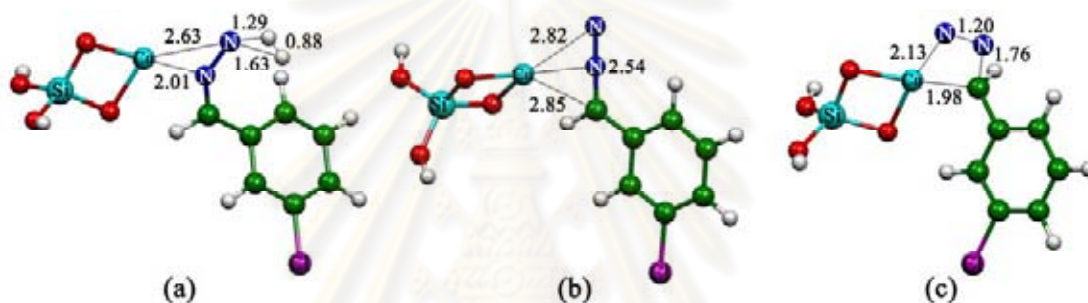
Figure 4.11 The B3LYP/LanL2DZ–optimized transition–state structures for dehydrogenation and denitrogenation to form olefinic intermediate in 3CBD reactant system (a) TS3_B, (b) TS4_B and (c) TS5_B. Bond distances are in Å.
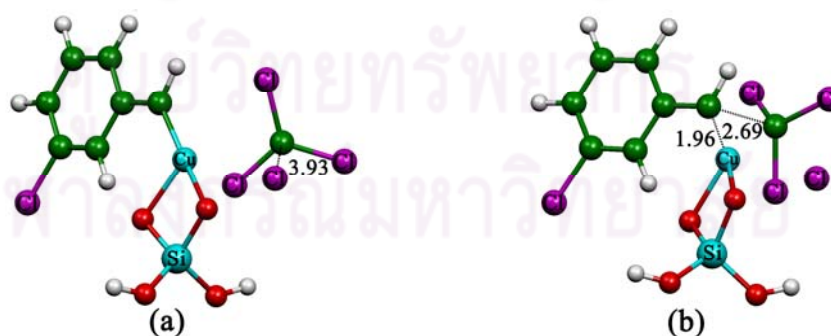
Figure 4.12 The B3LYP/LanL2DZ–optimized transition–state structures for chlorination of olefinic intermediate with CCl_4 to form the complex of DCV3CB product and dichloro Cu–pillared clay catalyst (a) TS6_B and (b) TS7_B. Bond distances are in Å.

Table 4.6 Imaginary frequencies for transition states of the DCV3CB product

transition state	imaginary frequency, cm^{-1}
TS1_B	−1434.23
TS2_B	−483.11
TS3_B	−1237.12
TS4_B	−134.03
TS5_B	−332.61
TS6_B	−333.61
TS7_B	−53.36

Table 4.7 Reaction energies, thermodynamic properties, rate and equilibrium constants for synthetic reaction of DCV3CB product in gas phase

Reaction	$\Delta^{\ddagger}E$ [a,b]	$\Delta^{\ddagger}G$ [a,b]	k_{298} [c]	ΔE [a]	ΔH_{298} [a]	ΔG_{298} [a]	K_{298}
Precursor formation:							
1B + HZ → [1B···HZ]	–	–	–	− 2.33	− 1.81	5.16	1.64 x 10^{-4}
[1B···HZ] →TS1_B → 3B	28.12	31.68	9.29 x 10^{-11}	− 2.64	− 3.94	0.98	1.09 x 10^{-1}
3B → TS2_B → [W···5B]	38.87	38.77	3.15 x 10^{-16}	− 8.84	− 8.08	− 10.01	2.17 x 10^{7}
[W···5B] → W + 5B	–	–	–	8.79	9.30	0.38	5.25 x 10^{-1}
Dehydrodenitrogenation:							
5B + Cat[d] → [5B···Cat]	–	–	–	− 39.18	− 38.42	− 27.91	2.88 x 10^{20}
[5B···Cat] → TS3_B → [H$_2$···8B]	89.06	88.67	1.52 x 10^{-52}	39.03	40.81	34.76	3.27 x 10^{-26}
[H$_2$···8B] → H$_2$ + 8B	–	–	–	− 0.19	0.10	− 5.02	4.82 x 10^{3}
8B → TS4_B → 9B	20.32	20.93	2.51 x 10^{-3}	6.19	6.10	7.76	2.04 x 10^{-6}
9B → TS5_B → [N$_2$···11B]	35.43	36.20	1.96 x 10^{-14}	− 4.79	− 3.85	− 6.62	7.16 x 10^{4}
[N$_2$···11B] → N$_2$ + 11B	–	–	–	4.14	3.77	− 2.93	1.41 x 10^{2}
Chlorination :							
11B + CCl$_4$ → [11B···CCl$_4$]	–	–	–	− 2.75	− 1.78	3.77	1.73 x 10^{-3}
[11B···CCl$_4$] → TS6_B → 13B	38.40	36.54	1.59 x 10^{-14}	35.07	35.57	33.47	2.92 x 10^{-25}
13B → TS7_B → 14B	1.77	6.36	1.12 x 10^{8}	− 53.56	− 54.15	− 50.54	1.12 x 10^{37}
14B → 15B[e]	–	–	–	− 14.22	− 14.18	− 13.23	4.97 x 10^{9}

[a] In kcal/mol.

[b] Activation state.

[c] Computed using Eq. 2.28, in s^{-1}.

[d] Cu–pillared clay catalyst.

[e] The complex of 1–(2,2–dichlorovinyl)–3–chlorobenzene (DCV3CB) with the dichloro Cu–pillared clay catalyst.

Table 4.7 shows that free energies of reaction steps, **3B → TS2_B → [W···5B], 5B + Cat → [5B···Cat], [H$_2$···8B] → H$_2$ + 8B, 9B → TS5_B → [N$_2$···11B], [N$_2$···11B] → N$_2$ + 11B, 13B → TS7_B → 14B** and **14B → 15B** are spontaneous reactions but the other reaction are non–spontaneous. The reaction steps, **1B + HZ → [1B···HZ], [1B···HZ] → TS1_B → 3B, 3B → TS2_B → [W···5B], 5B + Cat → [5B···Cat], 9B → TS5_B → [N$_2$···11B], 11B + CCl$_4$ → [11B···CCl$_4$], 13B → TS7_B → 14B** and **14B → 15B** are found to be an exothermic reaction. The magnitudes of

rate constants of all reaction steps are in order: **13B → TS7_B → 14B** (1.12 x 10^8 s^{-1}) > **8B → TS4_B → 9B** (2.51 x 10^{-3} s^{-1}) > **[1B···HZ] → TS1_B → 3B** (9.29 x 10^{-11} s^{-1}) > **[11B···CCl$_4$] → TS6_B → 13B** (1.59 x 10^{-14} s^{-1}) > **9B → TS5_B → [N$_2$···11B]** (1.96 x 10^{-14} s^{-1}) > **3B → TS2_B → [W···5B]** (3.15 x 10^{-16} s^{-1}) > **[5B···Cat] → TS3_B → [H$_2$···8B]** (1.52 x 10^{-52} s^{-1}). Rate–determining step is the **[5B···Cat] → TS3_B → [H$_2$···8B]** which is transition state of dehydrogenation because the slowest rate constants compared with all reaction steps.

Activation energies, tunneling coefficients, A factors and rate constants for synthetic reaction of DCV3CB product are shown in Table 4.8. The pre–exponential parameters (κ.A) are acceptable values as compare with any exponential results.

Table 4.8 Activation energies, tunneling coefficients, A factors and rate constants for synthetic reaction of DCV3CB product, computed at the B3LYP/LanL2DZ in gas phase

Reaction	κ^a	Q_{TS}/Q_{REA}	A^b	$\Delta^{\ddagger}E^c$	$k_{298}{}^d$
Precursor formation:					
1B + HZ → [1B···HZ]	–	–	–	–	–
[1B···HZ] →TS1_B → 3B	3.00	2.06 x 10^{-3}	1.28 x 10^{10}	28.12	9.29 x 10^{-11}
3B → TS2_B → [W···5B]	1.23	1.29 x 10^0	8.00 x 10^{12}	38.87	3.15 x 10^{-16}
[W···5B] → W + 5B	–	–	–	–	–
Dehydrodenitrogenation:					
5B + Cat^e → [5B···Cat]	–	–	–	–	–
[5B···Cat] → TS3_B → [H$_2$···8B]	2.49	1.92 x 10^0	1.19 x 10^{13}	89.06	1.52 x 10^{-52}
[H$_2$···8B] → H$_2$ + 8B	–	–	–	–	–
8B → TS4_B → 9B	1.02	3.10 x 10^{-1}	1.92 x 10^{12}	20.32	2.51 x 10^{-3}
9B → TS5_B → [N$_2$···11B]	1.11	2.69 x 10^{-1}	1.67 x 10^{12}	35.43	1.96 x 10^{-14}
[N$_2$···11B] → N$_2$ + 11B	–	–	–	–	–
Chlorination :					
11B + CCl$_4$ → [11B···CCl$_4$]	–	–	–	–	–
[11B···CCl$_4$] → TS6_B → 13B	1.11	3.28 x 10^1	2.04 x 10^{14}	38.40	1.59 x 10^{-14}
13B → TS7_B → 14B	1.00	3.54 x 10^{-4}	2.20 x 10^9	1.77	1.12 x 10^8
14B → 15B^f	–	–	–	–	–

^{a} $\kappa = 1 + \dfrac{1}{24}\left(\dfrac{h\nu_i}{k_BT}\right)^2$.

^{b} A = $\dfrac{k_BT}{h}\dfrac{Q_{TS}}{Q_{REA}}$, in s^{-1}.

^{c} Computed with ZPVE corrections, in kcal/mol.

^{d} Computed using Eq. 2.28, in s^{-1}.

^{e} Cu–pillared clay catalyst.

^{f} The complex of 1–(2,2–dichlorovinyl)–3–chlorobenzene (DCV3CB) with the dichloro Cu–pillared clay catalyst.

4.3 Reaction mechanism of olefination of 4BBD to DCV4BB product

      The potential energy profiles for the reaction of 4BBD and hydrazine to form DCV4BB product are shown in Figures 4.13–4.15; their transition–state structures are shown in Figures 4.16–4.18 and their imaginary frequencies are shown in Table 4.9. Reaction energies, thermodynamic properties, rate and equilibrium constants for synthetic reaction of DCV4BB product in gas phase are shown in Table 4.10.
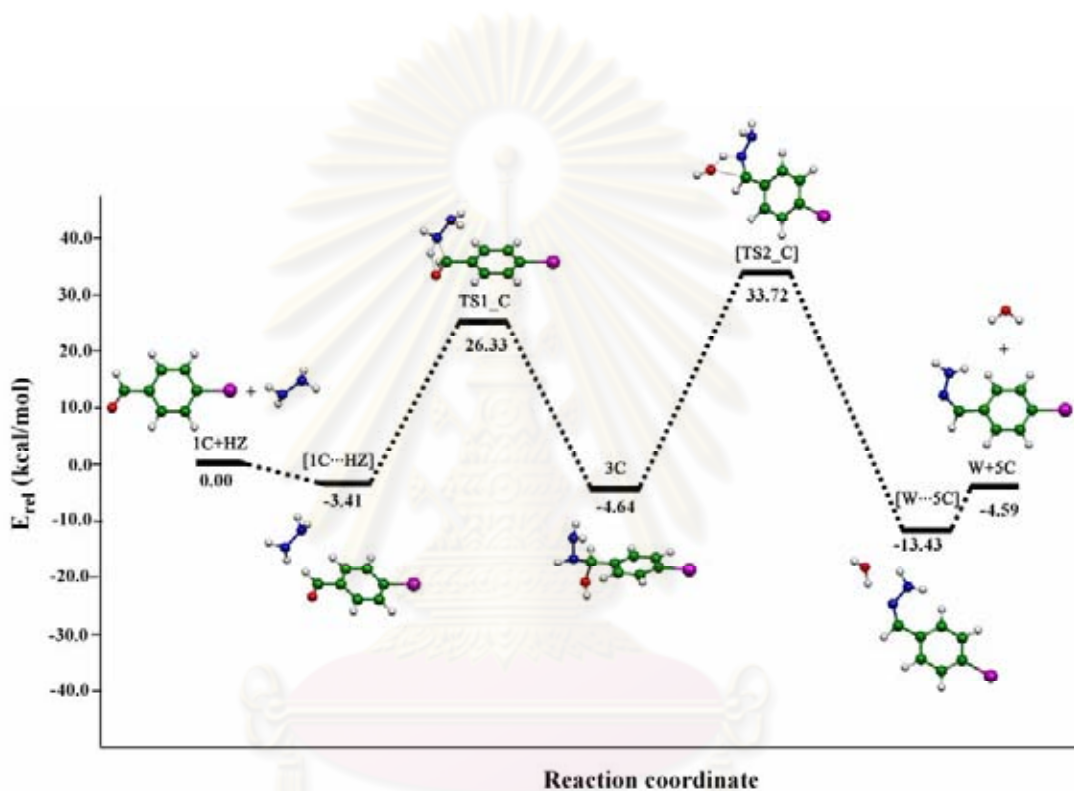
Figure 4.13 Potential energy profile for precursor formation of 4BBD and hydrazine to form hydrazone.
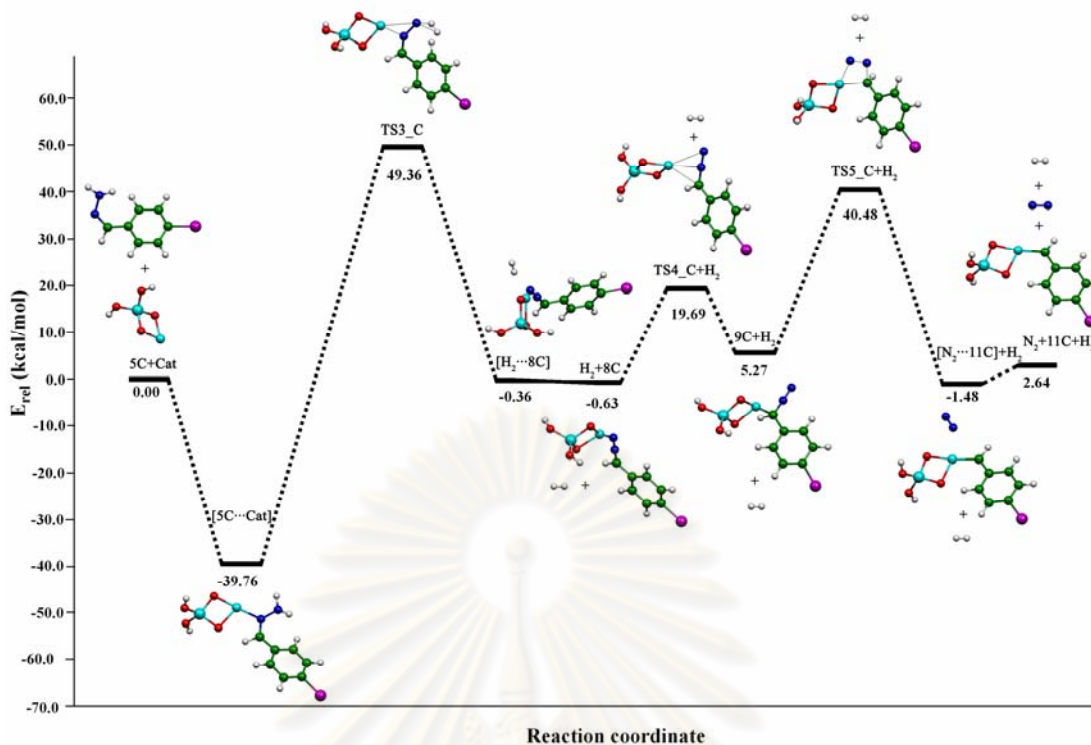
Figure 4.14 Potential energy profile for dehydrogenation and denitrogenation to form olefinic intermediate in 4BBD reactant system.
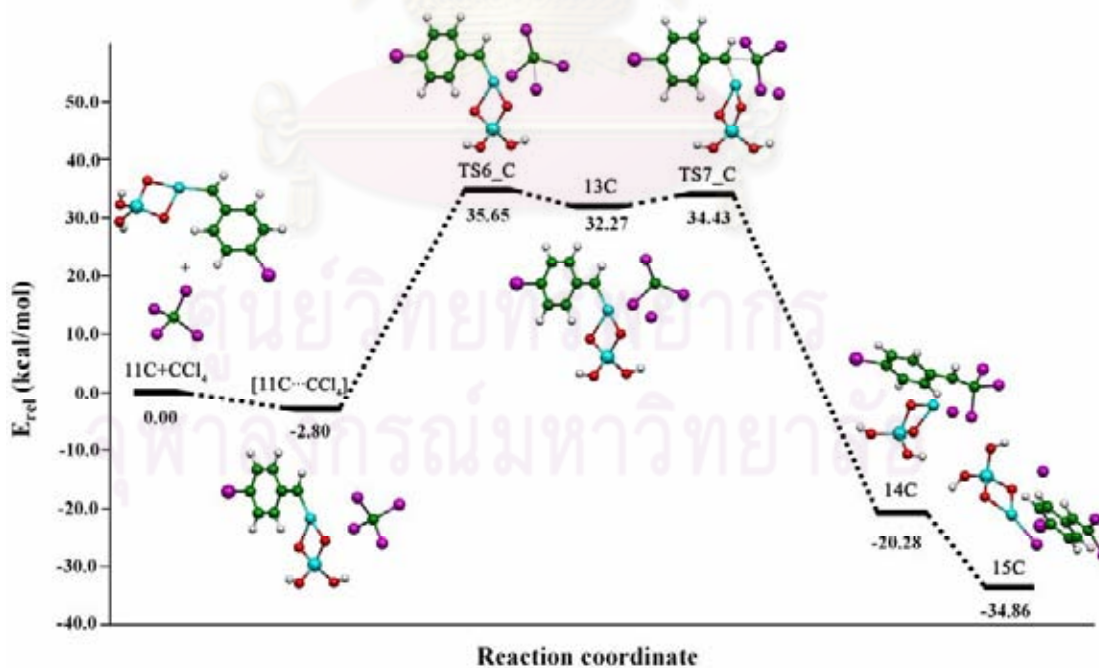
Figure 4.15 Potential energy profile for the chlorination of olefinic intermediate with CCl_4 to form the complex of DCV4BB product and the dichloro Cu–pillared clay catalyst.
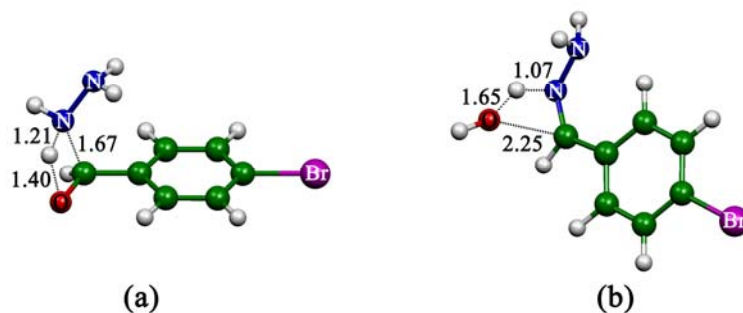
Figure 4.16 The B3LYP/LanL2DZ–optimized transition–state structures for precursor formation of 4BBD and hydrazine to form hydrazone (a) TS1_C and (b) TS2_C. Bond distances are in Å.
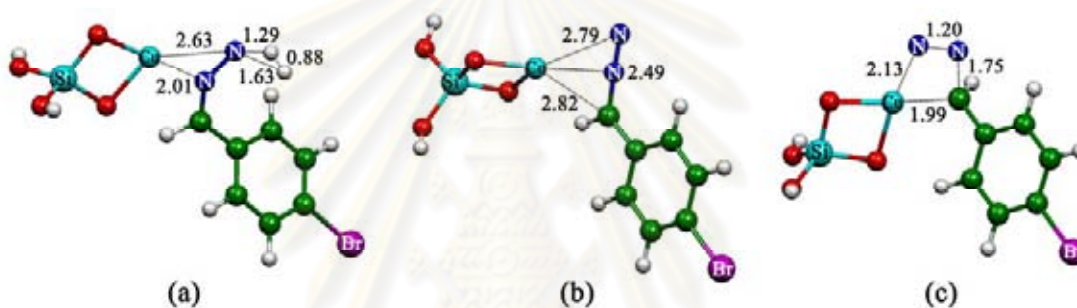
Figure 4.17 The B3LYP/LanL2DZ–optimized transition–state structures for dehydrogenation and denitrogenation to form olefinic intermediate in 4BBD reactant system (a) TS3_C, (b) TS4_C and (c) TS5_C. Bond distances are in Å.
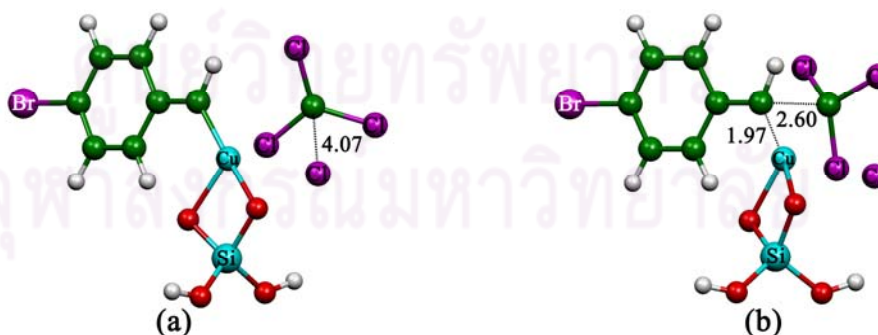
Figure 4.18 The B3LYP/LanL2DZ–optimized transition–state structures for chlorination of olefinic intermediate with CCl$_4$ to form the complex of DCV4BB product and dichloro Cu–pillared clay catalyst (a) TS6_C and (b) TS7_C. Bond distances are in Å.

Table 4.9 Imaginary frequencies for transition states of the DCV4BB product

transition state	imaginary frequency, cm^{-1}
TS1_C	–1430.30
TS2_C	–471.28
TS3_C	–1237.22
TS4_C	–133.75
TS5_C	–336.93
TS6_C	–335.60
TS7_C	–86.52

Table 4.10 Reaction energies, thermodynamic properties, rate and equilibrium constants for synthetic reaction of DCV4BB product in gas phase

Reaction	$\Delta^{\ddagger}E$ [a,b]	$\Delta^{\ddagger}G$ [a,b]	k_{298} [c]	ΔE [a]	ΔH_{298} [a]	ΔG_{298} [a]	K_{298}
Precursor formation:							
1C + HZ → [1C···HZ]	–	–	–	– 3.41	– 2.96	4.73	3.44 x 10^{-4}
[1C···HZ] →TS1_C → 3C	29.73	32.61	1.53 x 10^{-11}	– 1.23	– 2.42	1.69	5.77 x 10^{-2}
3C → TS2_C → [W···5C]	38.35	38.35	6.09 x 10^{-16}	– 8.80	– 8.03	– 9.97	2.04 x 10^{7}
[W···5C] → W + 5C	–	–	–	8.84	9.32	0.50	4.27 x 10^{-1}
Dehydrodenitrogenation:							
5C + Cat[d] → [5C···Cat]	–	–	–	– 39.76	– 39.02	– 28.32	5.72 x 10^{20}
[5C···Cat] → TS3_C → [H$_2$···8C]	89.12	88.50	2.04 x 10^{-52}	39.39	41.17	34.46	5.46 x 10^{-26}
[H$_2$···8C] → H$_2$ + 8C	–	–	–	– 0.26	0.04	– 4.68	2.71 x 10^{3}
8C → TS4_C → 9C	20.31	21.17	1.61 x 10^{-3}	5.89	5.84	7.50	3.17 x 10^{-6}
9C → TS5_C → [N$_2$···11C]	35.22	36.22	1.88 x 10^{-14}	– 6.75	– 5.82	– 8.52	1.75 x 10^{6}
[N$_2$···11C] → N$_2$ + 11C	–	–	–	4.12	3.76	– 2.97	1.51 x 10^{2}
Chlorination :							
11C + CCl$_4$ → [11C···CCl$_4$]	–	–	–	– 2.80	– 1.87	4.42	5.74 x 10^{-4}
[11C···CCl$_4$] → TS6_C → 13C	38.45	36.67	1.41 x 10^{-14}	35.08	35.57	33.59	2.38 x 10^{-25}
13C → TS7_C → 14C	2.16	5.84	2.76 x 10^{8}	– 52.55	– 53.14	– 49.20	1.16 x 10^{36}
14C → 15C[e]	–	–	–	– 14.58	– 14.49	– 14.86	7.83 x 10^{10}

[a] In kcal/mol.

[b] Activation state.

[c] Computed using Eq. 2.28, in s^{-1}.

[d] Cu–pillared clay catalyst.

[e] The complex of 1–(2,2–dichlorovinyl)–4–bromobenzene (DCV4BB) with the dichloro Cu–pillared clay catalyst.

Table 4.10 shows that free energies of reaction steps, **3C → TS2_C → [W···5C]**, **5C + Cat → [5C···Cat]**, **[H$_2$···8C] → H$_2$ + 8C**, **9C → TS5_C → [N$_2$···11C]**, **[N$_2$···11C] → N$_2$ + 11C**, **13C → TS7_C → 14C** and **14C → 15C** are spontaneous reactions but the other reaction are non–spontaneous. The reaction steps, **1C + HZ → [1C···HZ]**, **[1C···HZ] →TS1_C → 3C**, **3C → TS2_C → [W···5C]**, **5C + Cat → [5C···Cat]**, **9C → TS5_C → [N$_2$···11C]**, **11C + CCl$_4$ → [11C···CCl$_4$]**, **13C → TS7_C → 14C** and **14C → 15C** are found to be an exothermic reaction. The

magnitudes of rate constants of all reaction steps are in order: **13C → TS7_C → 14C** (2.76 x 10^8 s^{-1}) > **8C → TS4_C → 9C** (1.61 x 10^{-3} s^{-1}) > **[1C···HZ] → TS1_C → 3C** (1.53 x 10^{-11} s^{-1}) > **[11C···CCl$_4$] → TS6_C → 13C** (1.41 x 10^{-14} s^{-1}) > **9C → TS5_C → [N$_2$···11C]** (1.88 x 10^{-14} s^{-1}) > **3C → TS2_C → [W···5C]** (6.09 x 10^{-16} s^{-1}) > **[5C···Cat] → TS3_C → [H$_2$···8C]** (2.04 x 10^{-52} s^{-1}). Rate–determining step is the **[5C···Cat] → TS3_C → [H$_2$···8C]** which is transition state of dehydrogenation because the slowest rate constants compared with all reaction step.

Activation energies, tunneling coefficients, A factors and rate constants for synthetic reaction of DCV4BB product are shown in Table 4.11. The pre–exponential parameters (κ.A) are acceptable values as compare with any exponential results.

Table 4.11 Activation energies, tunneling coefficients, A factors and rate constants for synthetic reaction of DCV4BB product, computed at the B3LYP/LanL2DZ in gas phase

Reaction	κ^a	Q_{TS}/Q_{REA}	A^b	$\Delta^{\ddagger}E^c$	$k_{298}{}^d$
Precursor formation:					
1C + HZ → [1C···HZ]	–	–	–	–	–
[1C···HZ] →TS1_C → 3C	2.99	5.19 x 10^{-3}	3.22 x 10^{10}	29.73	1.53 x 10^{-11}
3C → TS2_C → [W···5C]	1.22	1.06 x 10^0	6.56 x 10^{12}	38.35	6.09 x 10^{-16}
[W···5C] → W + 5C	–	–	–	–	–
Dehydrodenitrogenation:					
5C + Cat^e → [5C···Cat]	–	–	–	–	–
[5C···Cat] → TS3_C → [H$_2$···8C]	2.49	2.83 x 10^0	1.76 x 10^{13}	89.12	2.04 x 10^{-52}
[H$_2$···8C] → H$_2$ + 8C	–	–	–	–	–
8C → TS4_C → 9C	1.02	1.98 x 10^{-1}	1.23 x 10^{12}	20.31	1.61 x 10^{-3}
9C → TS5_C → [N$_2$···11C]	1.11	1.78 x 10^{-1}	1.11 x 10^{12}	35.22	1.88 x 10^{-14}
[N$_2$···11C] → N$_2$ + 11C	–	–	–	–	–
Chlorination :					
11C + CCl$_4$ → [11C···CCl$_4$]	–	–	–	–	–
[11C···CCl$_4$] → TS6_C → 13C	1.11	3.16 x 10^1	1.96 x 10^{14}	38.45	1.41 x 10^{-14}
13C → TS7_C → 14C	1.01	1.68 x 10^{-3}	1.04 x 10^{10}	2.16	2.76 x 10^8
14C → 15C^f	–	–	–	–	–

^{a} $\kappa = 1 + \dfrac{1}{24}\left(\dfrac{h\nu_i}{k_BT}\right)^2$.

^{b} A $= \dfrac{k_BT}{h}\dfrac{Q_{TS}}{Q_{REA}}$, in s^{-1}.

^{c} Computed with ZPVE corrections, in kcal/mol.

^{d} Computed using Eq. 2.28, In s^{-1}.

^{e} Cu–pillared clay catalyst.

^{f} The complex of 1–(2,2–dichlorovinyl)–4–bromobenzene (DCV4BB) with the dichloro Cu–pillared clay catalyst.

4.4 Reaction mechanism of olefination of 3BBD to DCV3BB product

The potential energy profiles for the reaction of 3BBD and hydrazine to form DCV3BB product are shown in Figures 4.19–4.21 their transition–state structures are shown in Figures 4.22–4.24 and their imaginary frequencies are shown in Table 4.12. Reaction energies, thermodynamic properties, rate and equilibrium constants for synthetic reaction of DCV3BB product in gas phase are shown in Table 4.13.
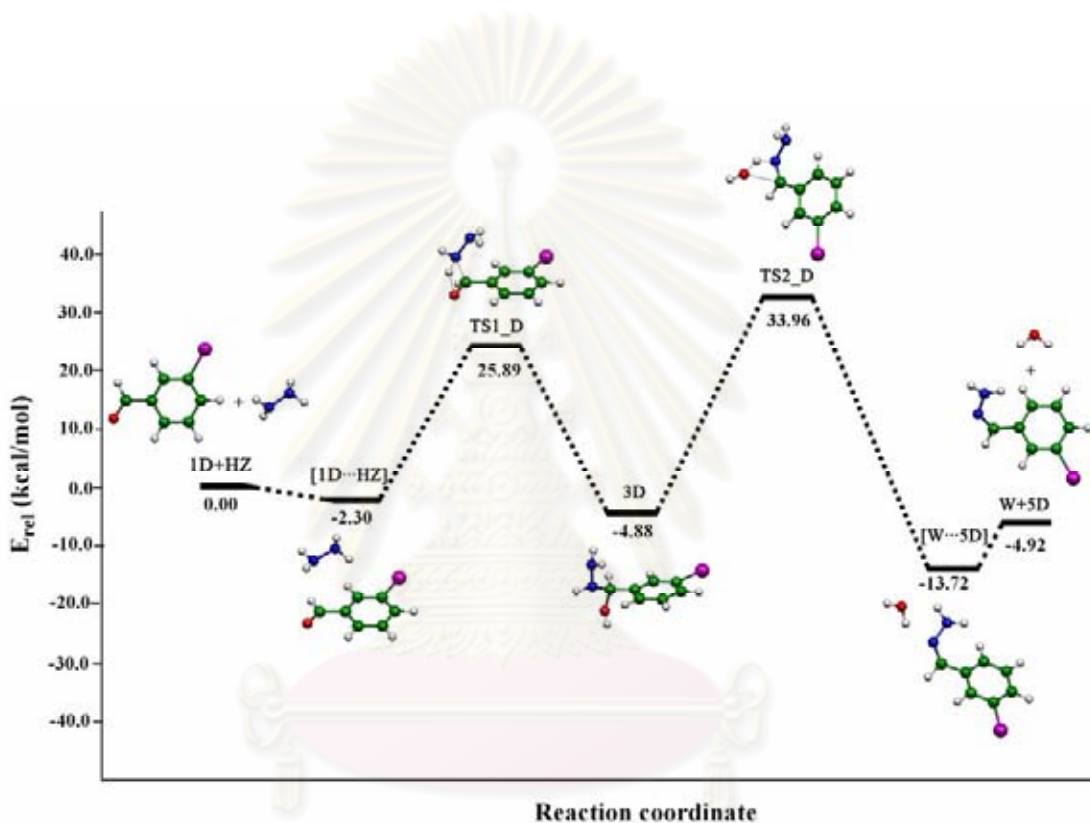
Figure 4.19 Potential energy profile for precursor formation of 3BBD and hydrazine to form hydrazone.
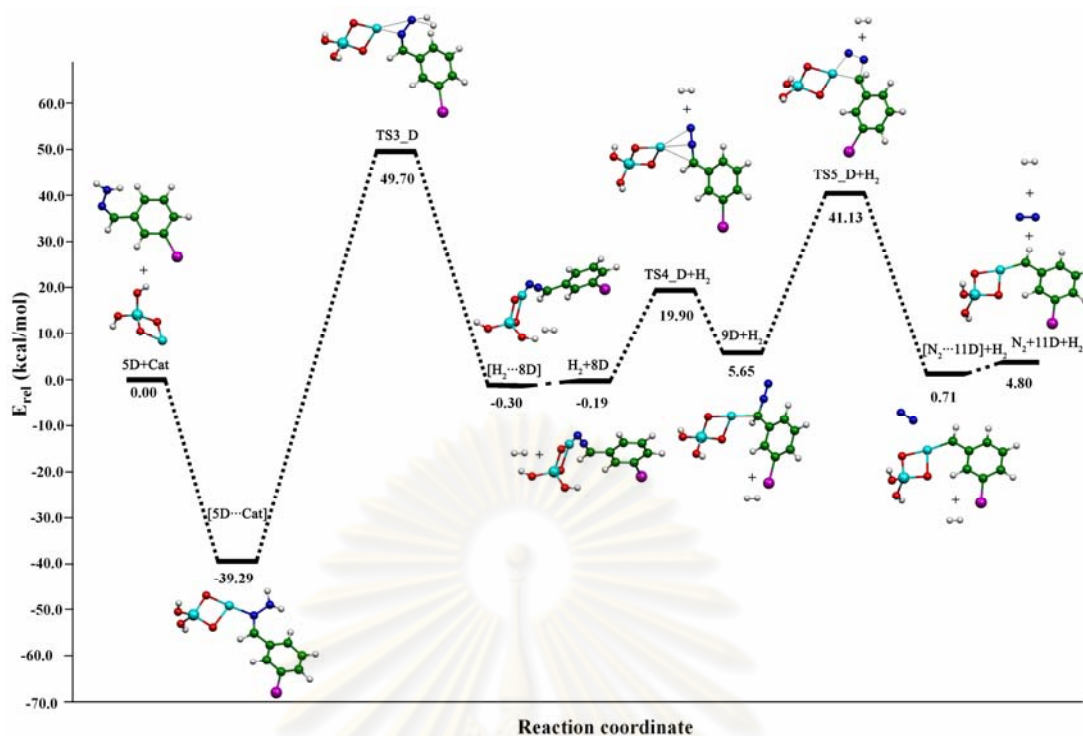
Figure 4.20 Potential energy profile for dehydrogenation and denitrogenation to form olefinic intermediate in 3BBD reactant system.
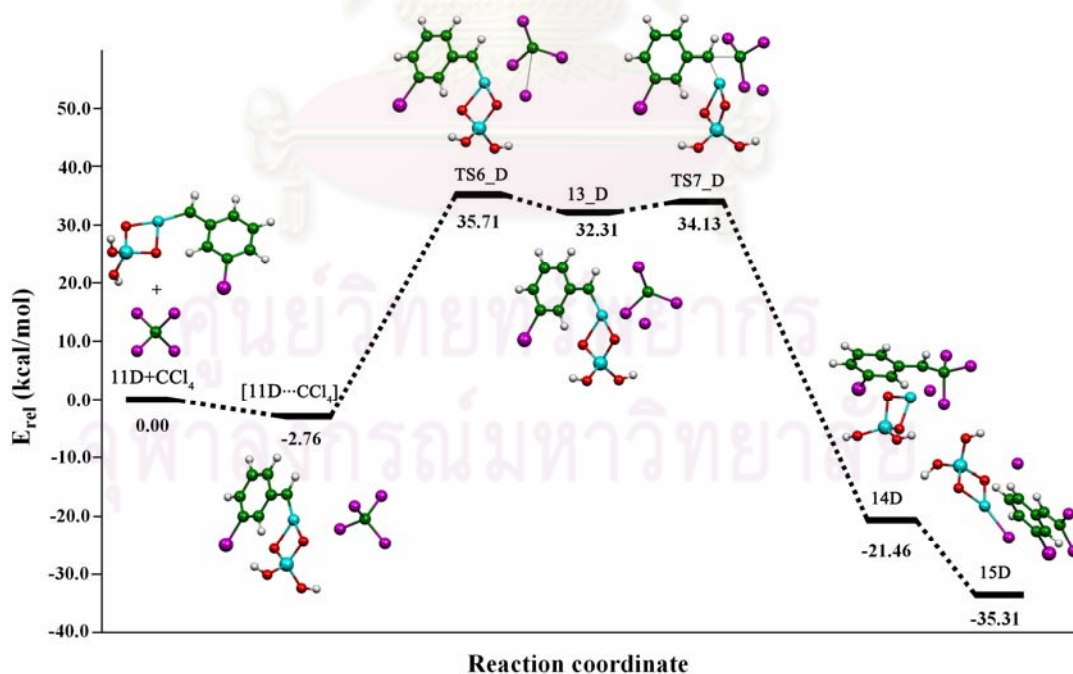
Figure 4.21 Potential energy profile for the chlorination of olefinic intermediate with CCl_4 to form the complex of DCV3BB product and the dichloro Cu–pillared clay catalyst.
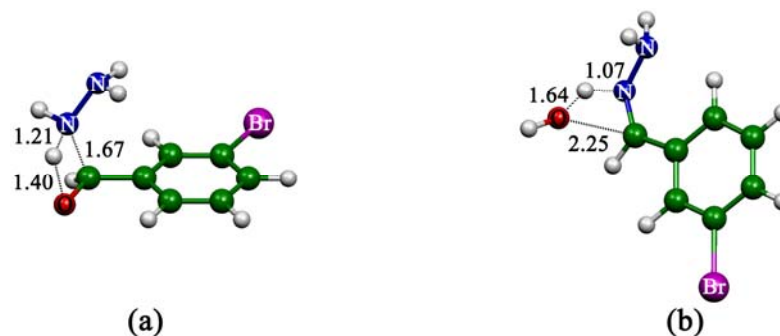
Figure 4.22 The B3LYP/LanL2DZ–optimized transition–state structures for precursor formation of 3BBD and hydrazine to form hydrazone (a) TS1_D and (b) TS2_D. Bond distances are in Å.
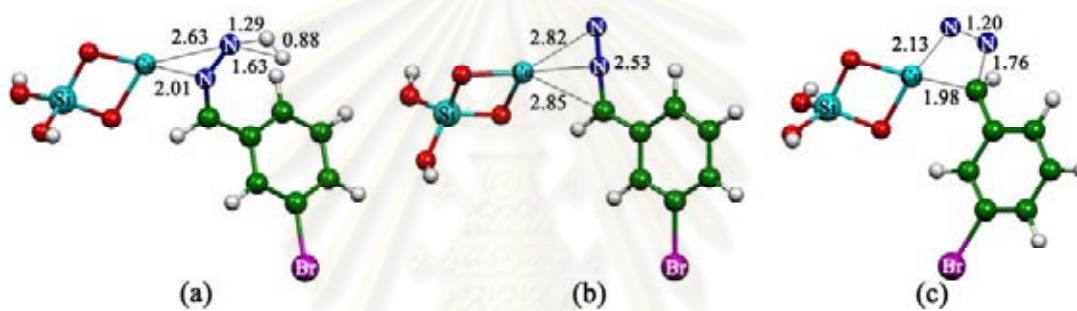
Figure 4.23 The B3LYP/LanL2DZ–optimized transition–state structures for dehydrogenation and denitrogenation to form olefinic intermediate in 3BBD reactant system (a) TS3_D, (b) TS4_D and (c) TS5_D. Bond distances are in Å.
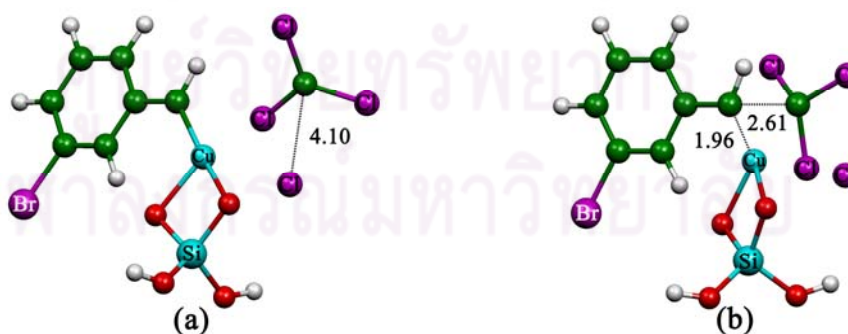
Figure 4.24 The B3LYP/LanL2DZ–optimized transition–state structures for chlorination of olefinic intermediate with CCl_4 to form the complex of DCV3BB product and dichloro Cu–pillared clay catalyst (a) TS6_D and (b) TS7_D. Bond distances are in Å.

Table 4.12 Imaginary frequencies for transition states of the DCV3BB product

transition state	imaginary frequency, cm^{-1}
TS1_D	−1433.37
TS2_D	−471.17
TS3_D	−1238.30
TS4_D	−131.18
TS5_D	−332.35
TS6_D	−335.65
TS7_D	−81.39

Table 4.13 Reaction energies, thermodynamic properties, rate and equilibrium constants for synthetic reaction of DCV3BB product in gas phase

| Reaction	$\Delta^{\ddagger}E$ [a,b]	$\Delta^{\ddagger}G$ [a,b]	k_{298} [c]	ΔE [a]	ΔH_{298} [a]	ΔG_{298} [a]	K_{298}
Precursor formation:							
1D + HZ → [1D···HZ]	–	–	–	− 2.30	− 1.78	5.27	1.38 x 10^{-4}
[1D···HZ] →TS1_D → 3D	28.20	31.68	9.56 x 10^{-11}	− 2.58	− 3.88	0.98	1.92 x 10^{-1}
3D → TS2_D → [W···5D]	38.85	38.73	3.31 x 10^{-16}	− 8.84	− 8.06	− 10.04	2.28 x 10^{7}
[W···5D] → W + 5D	–	–	–	8.80	9.30	0.40	5.90 x 10^{-1}
Dehydrodenitrogenation:							
5D + Cat[d] → [5D···Cat]	–	–	–	− 39.29	− 38.55	− 27.90	2.82 x 10^{20}
[5D···Cat] → TS3_D → [H$_2$···8D]	88.99	88.35	2.61 x 10^{-52}	38.99	40.81	34.44	5.66 x 10^{-26}
[H$_2$···8D] → H$_2$ + 8D	–	–	–	0.11	0.31	− 4.45	1.83 x 10^{3}
8D → TS4_D → 9D	20.09	20.75	3.38 x 10^{-3}	5.84	5.90	6.86	9.29 x 10^{-6}
9D → TS5_D → [N$_2$···11D]	35.48	36.77	7.53 x 10^{-15}	− 4.94	− 4.07	− 6.31	4.26 x 10^{4}
[N$_2$···11D] → N$_2$ + 11D	–	–	–	4.09	3.75	− 3.10	1.89 x 10^{2}
Chlorination :							
11D + CCl$_4$ → [11D···CCl$_4$]	–	–	–	− 2.76	− 1.81	3.81	1.61 x 10^{-3}
[11D···CCl$_4$] → TS6_D → 13D	38.47	36.64	1.54 x 10^{-14}	35.07	35.56	33.67	2.07 x 10^{-25}
13D → TS7_D → 14D	1.82	6.66	6.82 x 10^{7}	− 53.76	− 54.39	− 49.57	2.17 x 10^{36}
14D→ 15D[e]	–	–	–	− 13.85	− 13.76	− 14.46	3.95 x 10^{10}

[a] In kcal/mol.

[b] Activation state.

[c] Computed using Eq. 2.28, in s^{-1}.

[d] Cu–pillared clay catalyst.

[e] The complex of 1–(2,2–dichlorovinyl)–3–bromobenzene (DCV3BB) with the dichloro Cu–pillared clay catalyst.

Table 4.13 shows that free energies of reaction steps, **3D → TS2_D → [W···5D], 5D + Cat → [5D···Cat], [H$_2$···8D] → H$_2$ + 8D, 9D → TS5_D → [N$_2$···11D], [N$_2$···11D] → N$_2$ + 11D, 13D → TS7_D → 14D** and **14D → 15D** are spontaneous reactions but the other reaction are non–spontaneous. The reaction steps, **1D + HZ → [1D···HZ], [1D···HZ] →TS1_D → 3D, 3D → TS2_D → [W···5D], 5D + Cat → [5D···Cat], 9D → TS5_D → [N$_2$···11D], 11D + CCl$_4$ → [11D···CCl$_4$], 13D**

→ **TS7_D** → **14D** and **14D** → **15D** are found to be an exothermic reaction. The magnitudes of rate constants of all reaction steps are in order: **13D** → **TS7_D** → **14D** (6.82×10^7 s^{-1}) > **8D** → **TS4_D** → **9D** (3.38×10^{-3} s^{-1}) > **[1D···HZ]** → **TS1_D** → **3D** (9.56×10^{-11} s^{-1}) > **[11D···CCl$_4$]** → **TS6_D** → **13D** (1.54×10^{-14} s^{-1}) > **9D** → **TS5_D** → **[N$_2$···11D]** (7.53×10^{-15} s^{-1}) > **3D** → **TS2_D** → **[W···5D]** (3.31×10^{-16} s^{-1}) > **[5D···Cat]** → **TS3_D** → **[H$_2$···8D]** (2.61×10^{-52} s^{-1}). Rate–determining step is the **[5D···Cat]** → **TS3_D** → **[H$_2$···8D]** which is transition state of dehydrogenation because the slowest rate constants compared with all reaction steps.

Activation energies, tunneling coefficients, A factors and rate constants for synthetic reaction of DCV3BB product are shown in Table 4.14. The pre–exponential parameters (κ.A) are acceptable values as compare with any exponential results.

Table 4.14 Activation energies, tunneling coefficients, A factors and rate constants for synthetic reaction of DCV3BB product, computed at the B3LYP/LanL2DZ in gas phase

Reaction	κ[a]	Q_{TS}/Q_{REA}	A[b]	$\Delta^{\ddagger}E$[c]	k_{298}[d]
Precursor formation:					
1D + HZ → [1D···HZ]	–	–	–	–	–
[1D···HZ] →TS1_D → 3D	2.99	2.41×10^{-3}	1.50×10^{10}	28.20	9.56×10^{-11}
3D → TS2_D → [W···5D]	1.22	1.31×10^{0}	8.15×10^{12}	38.85	3.31×10^{-16}
[W···5D] → W + 5D	–	–	–	–	–
Dehydrodenitrogenation:					
5D + Cat[e] → [5D···Cat]	–	–	–	–	–
[5D···Cat] → TS3_D → [H$_2$···8D]	2.49	2.93×10^{0}	1.82×10^{13}	88.99	2.61×10^{-52}
[H$_2$···8D] → H$_2$ + 8D	–	–	–	–	–
8D → TS4_D → 9D	1.02	2.86×10^{-1}	1.78×10^{12}	20.09	3.38×10^{-3}
9D → TS5_D → [N$_2$···11D]	1.11	1.11×10^{-1}	6.91×10^{11}	35.48	7.53×10^{-15}
[N$_2$···11D] → N$_2$ + 11D	–	–	–	–	–
Chlorination :					
11D + CCl$_4$ → [11D···CCl$_4$]	–	–	–	–	–
[11D···CCl$_4$] → TS6_D → 13D	1.11	3.55×10^{1}	2.20×10^{14}	38.47	1.54×10^{-14}
13D → TS7_D → 14D	1.01	2.36×10^{-4}	1.47×10^{9}	1.82	6.82×10^{7}
14D → 15D[f]	–	–	–	–	–

[a] $\kappa = 1 + \dfrac{1}{24}\left(\dfrac{h\nu_i}{k_B T}\right)^2$.

[b] A $= \dfrac{k_B T}{h}\dfrac{Q_{TS}}{Q_{REA}}$, in s^{-1}.

[c] Computed with ZPVE corrections, in kcal/mol.

[d] Computed using Eq. 2.28, in s^{-1}.

[e] Cu– pillared clay catalyst.

[f] The complex of 1–(2,2–dichlorovinyl)–3–bromobenzene (DCV3BB) with the dichloro Cu– pillared clay catalyst.

4.5 Reaction mechanism of olefination of BD to DCVB

The potential energy profiles for the reaction of BD and hydrazine to form DCVB product are shown in Figures 4.25–4.27; their transition–state structures are shown in Figures 4.28–4.30 and their imaginary frequencies are shown in Table 4.15. Reaction energies, thermodynamic properties, rate and equilibrium constants for synthetic reaction of DCV3BB product in gas phase are shown in Table 4.16.
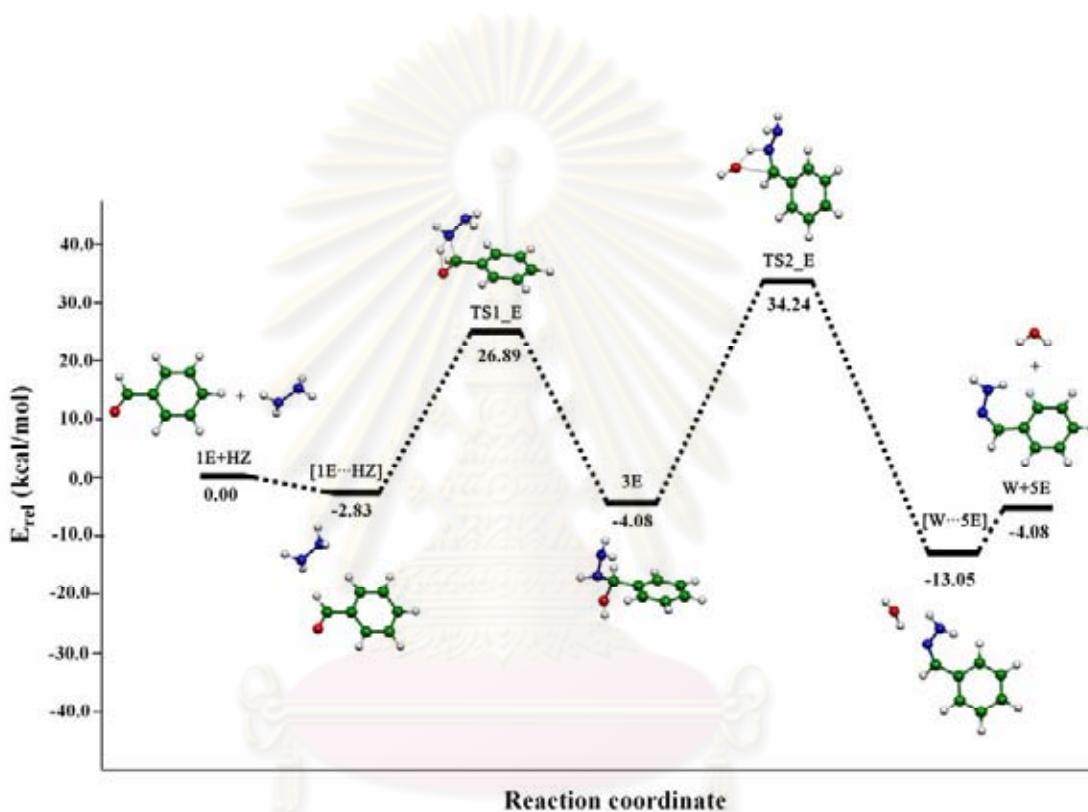
Figure 4.25 Potential energy profile for precursor formation of BD and hydrazine to form hydrazone.
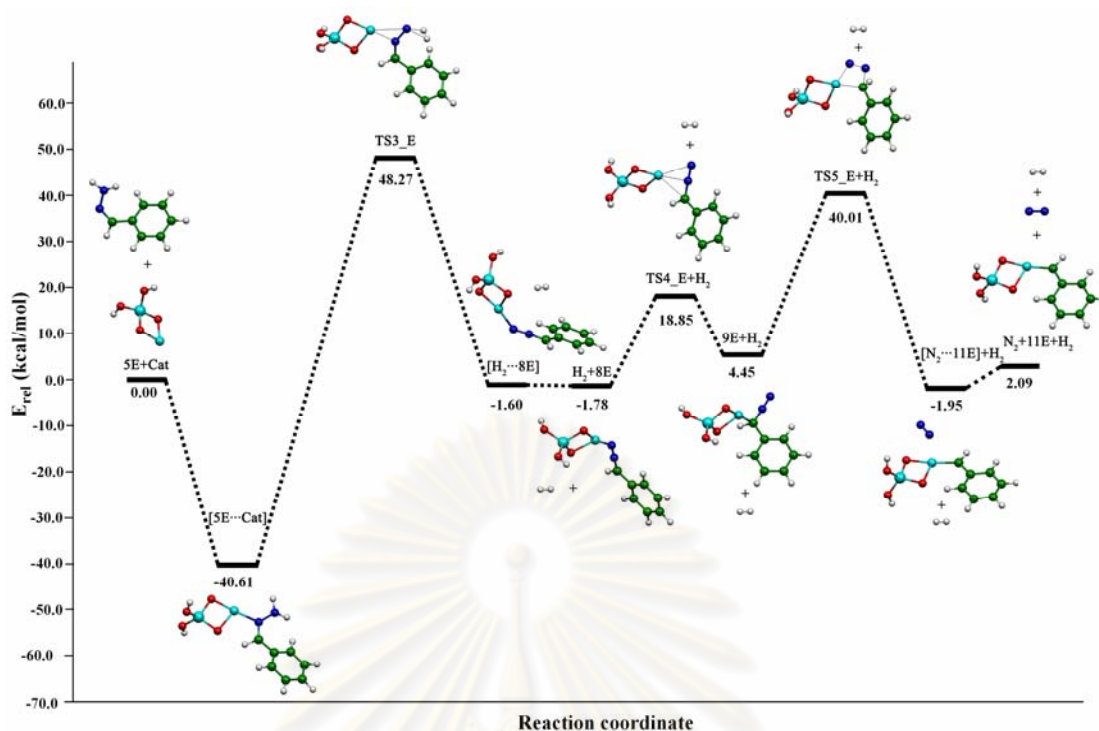
Figure 4.26 Potential energy profile for dehydrogenation and denitrogenation to form olefinic intermediate in BD reactant system.
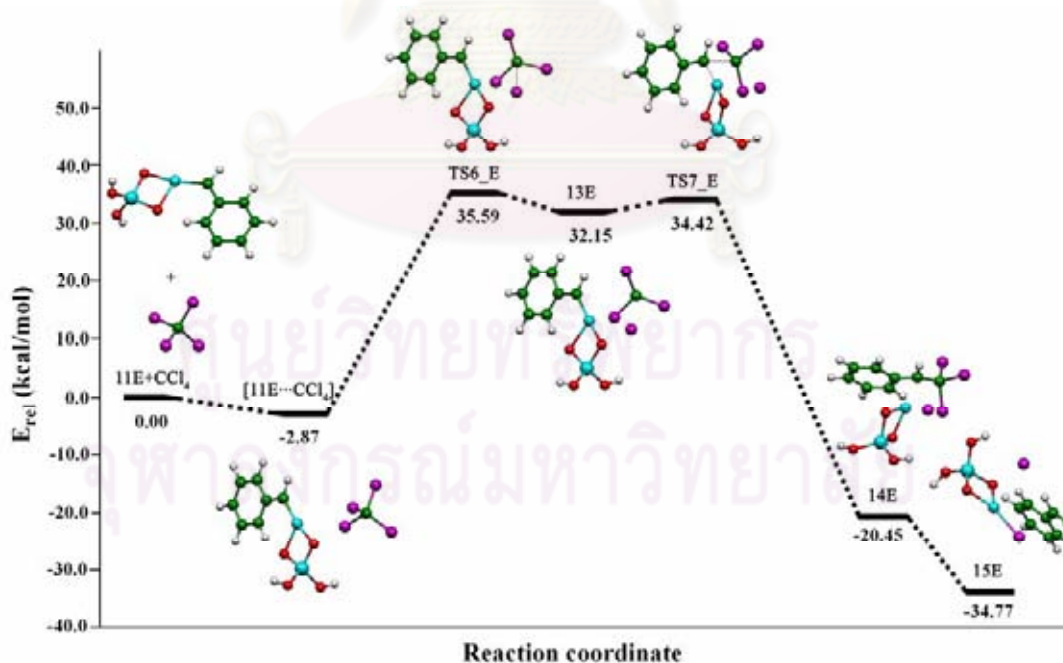
Figure 4.27 Potential energy profile for the chlorination of olefinic intermediate with CCl_4 to form the complex of DCVB product and the dichloro Cu–pillared clay catalyst.
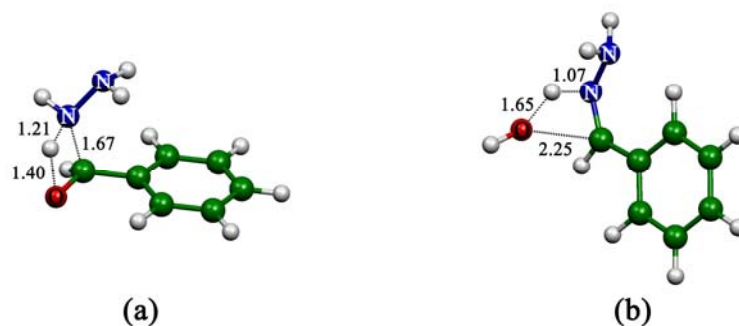
Figure 4.28 The B3LYP/LanL2DZ–optimized transition–state structures for precursor formation of BD and hydrazine to form hydrazone (a) TS1_E and (b) TS2_E. Bond distances are in Å.
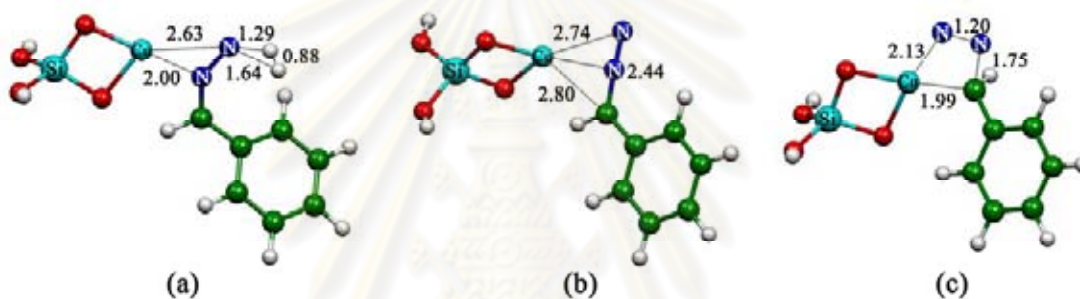
Figure 4.29 The B3LYP/LanL2DZ–optimized transition–state structures for dehydrogenation and denitrogenation to form olefinic intermediate in BD reactant system (a) TS3_E, (b) TS4_E and (c) TS5_E. Bond distances are in Å.
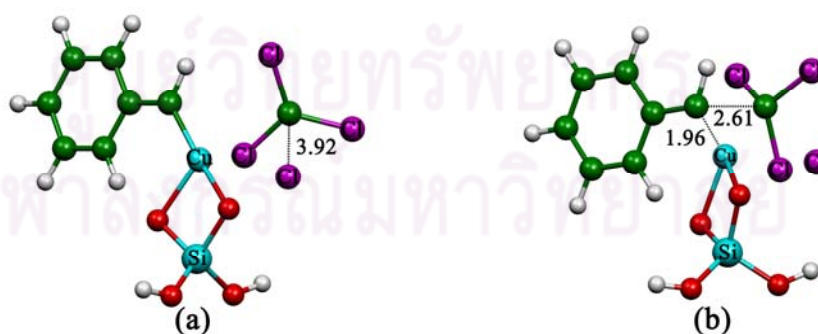
Figure 4.30 The B3LYP/LanL2DZ–optimized transition–state structures for chlorination of olefinic intermediate with CCl$_4$ to form the complex of DCVB product and dichloro Cu–pillared clay catalyst (a) TS6_E and (b) TS7_E. Bond distances are in Å.

Table 4.15 Imaginary frequencies for transition states of the DCVB product

transition state	imaginary frequency, cm^{-1}
TS1_E	−1427.03
TS2_E	−462.07
TS3_E	−1207.02
TS4_E	−138.05
TS5_E	−346.48
TS6_E	−334.48
TS7_E	−81.00

Table 4.16 Reaction energies, thermodynamic properties, rate and equilibrium constants for the synthetic reaction of DCVB product in gas phase

Reaction	$\Delta^{\ddagger}E$ [a,b]	$\Delta^{\ddagger}G$ [a,b]	k_{298} [c]	ΔE [a]	ΔH_{298} [a]	ΔG_{298} [a]	K_{298}
Precursor formation:							
1E + HZ → [1E···HZ]	–	–	–	− 2.83	− 2.33	4.94	2.39 x 10^{-4}
[1E···HZ] →TS1_E → 3E	29.71	32.95	7.81 x 10^{-12}	− 1.25	− 2.52	2.01	3.35 x 10^{-2}
3E → TS2_E → [W···5E]	38.32	38.32	6.73 x 10^{-16}	− 8.97	− 8.22	− 10.11	2.60 x 10^{7}
[W···5E] → W + 5E	–	–	–	8.97	9.48	0.62	3.50 x 10^{-1}
Dehydrodenitrogenation:							
5E + Cat[d] → [5E···Cat]	–	–	–	− 40.61	− 39.91	− 29.22	2.63 x 10^{21}
[5E···Cat] → TS3_E → [H$_2$···8E]	88.89	88.31	2.71 x 10^{-52}	39.01	40.92	33.22	4.42 x 10^{-25}
[H$_2$···8E] → H$_2$ + 8E	–	–	–	− 0.17	0.03	− 3.93	7.64 x 10^{2}
8E → TS4_E → 9E	20.63	21.75	5.96 x 10^{-4}	6.23	6.10	8.18	1.00 x 10^{-6}
9E → TS5_E → [N$_2$···11E]	35.56	35.30	1.64 x 10^{-14}	− 6.40	− 5.42	− 8.30	1.22 x 10^{6}
[N$_2$···11E] → N$_2$ + 11E	–	–	–	4.04	3.66	− 3.03	1.67 x 10^{2}
Chlorination :							
11E + CCl$_4$ → [11E···CCl$_4$]	–	–	–	− 2.87	− 1.93	3.99	1.20 x 10^{-3}
[11E···CCl$_4$] → TS6_E → 13E	38.46	36.84	9.81 x 10^{-15}	35.02	35.56	32.76	9.66 x 10^{-25}
13E → TS7_E → 14E	2.27	7.37	1.95 x 10^{7}	− 52.59	− 53.30	− 47.95	1.42 x 10^{35}
14E→ 15E[e]	–	–	–	− 14.33	− 14.20	− 14.73	6.25 x 10^{10}

[a] In kcal/mol.

[b] Activation state.

[c] Computed using Eq. 2.28, in s^{-1}.

[d] Cu–pillared clay catalyst.

[e] The complex of 1–(2,2–dichlorovinyl)–benzene (DCVB) with the dichloro Cu–pillared clay catalyst.

Table 4.16 shows that free energies of reaction steps, **3E → TS2_E → [W···5E], 5E + Cat → [5E···Cat], [H$_2$···8E] → H$_2$ + 8E, 9E → TS5_E → [N$_2$···11E], [N$_2$···11E] → N$_2$ + 11E, 13E → TS7_E → 14E** and **14E → 15E** are spontaneous reactions but the other reaction are non–spontaneous. The reaction steps, **1E + HZ → [1E···HZ], [1E···HZ] →TS1_E → 3E, 3E → TS2_E → [W···5E], 5E + Cat → [5E···Cat], 9E → TS5_E → [N$_2$···11E], 11E + CCl$_4$ → [11E···CCl$_4$], 13E → TS7_E → 14E** and **14E → 15E** are found to be an exothermic reaction. The magnitudes of

rate constants of all reaction steps are in order: **13E → TS7_E → 14E** (1.95 x 10^7 s^{-1}) > **8E → TS4_E → 9E** (5.96 x 10^{-4} s^{-1}) > **[1E···HZ] → TS1_E → 3E** (7.81 x 10^{-12} s^{-1}) > **9E → TS5_E → [N$_2$···11E]** (1.64 x 10^{-14} s^{-1}) > **[11E···CCl$_4$] → TS6_E → 13E** (9.81 x 10^{-15} s^{-1}) > **3E → TS2_E → [W···5E]** (6.73 x 10^{-16} s^{-1}) > **[5E···Cat] → TS3_E → [H$_2$···8E]** (2.71 x 10^{-52} s^{-1}). Rate–determining step is the **[5E···Cat] → TS3_E → [H$_2$···8E]** which is transition state of dehydrogenation because the slowest rate constants compared with all reaction steps.

Activation energies, tunneling coefficients, A factors and rate constants for synthetic reaction of DCVB product are shown in Table 4.17. The pre–exponential parameters (κ.A) are acceptable values as compare with any exponential results.

Table 4.17 Activation energies, tunneling coefficients, A factors and rate constants for the synthetic reaction of DCVB product, computed at the B3LYP/LanL2DZ in gas phase

Reaction	κ^a	Q_{TS}/Q_{REA}	A^b	$\Delta^{\ddagger}E^c$	$k_{298}{}^d$
Precursor formation:					
1E + HZ → [1E···HZ]	–	–	–	–	–
[1E···HZ] →TS1_E → 3E	2.98	2.56 x 10^{-3}	1.59 x 10^{10}	29.70	7.81 x 10^{-12}
3E → TS2_E → [W···5E]	1.21	1.10 x 10^0	6.85 x 10^{12}	38.32	6.73 x 10^{-16}
[W···5E] → W + 5E	–	–	–	–	–
Dehydrodenitrogenation:					
5E + Cat^e → [5E···Cat]	–	–	–	–	–
[5E···Cat] → TS3_E → [H$_2$···8E]	2.41	2.63 x 10^0	1.63 x 10^{13}	88.89	2.71 x 10^{-52}
[H$_2$···8E] → H$_2$ + 8E	–	–	–	–	–
8E → TS4_E → 9E	1.02	1.25 x 10^{-1}	7.78 x 10^{11}	20.63	5.96 x 10^{-4}
9E → TS5_E → [N$_2$···11E]	1.12	2.77 x 10^{-1}	1.72 x 10^{12}	35.56	1.64 x 10^{-14}
[N$_2$···11E] → N$_2$ + 11E	–	–	–	–	–
Chlorination :					
11E + CCl$_4$ → [11E···CCl$_4$]	–	–	–	–	–
[11E···CCl$_4$] → TS6_E → 13E	1.11	2.24 x 10^1	1.39 x 10^{14}	38.46	9.81 x 10^{-15}
13E → TS7_E → 14E	1.01	1.44 x 10^{-4}	8.95 x 10^8	2.27	1.95 x 10^7
14E→ 15E^f	–	–	–	–	–

^{a} $\kappa = 1 + \dfrac{1}{24}\left(\dfrac{h\nu_i}{k_BT}\right)^2$.

^{b} A $= \dfrac{k_BT}{h}\dfrac{Q_{TS}}{Q_{REA}}$, in s^{-1}.

^{c} Computed with ZPVE corrections, in kcal/mol.

^{d} Computed using Eq. 2.28, in s^{-1}.

^{e} Cu–pillared clay catalyst.

^{f} The complex of 1–(2,2–dichlorovinyl)–benzene (DCVB) with the dichloro Cu–pillared clay catalyst.

## 4.6 Reaction mechanism of recovery process of olefination

The potential energy profile for the recovery process of Cu–pillared clay catalyst is shown in Figure 4.31 and its transition–state structure is shown in Figure 4.32. The imaginary frequency of the transition state of the recovery process is shown in Table 4.18. The reaction energies, thermodynamic properties, rate and equilibrium constants for reactions in the recovery process in gas phase are shown in Table 4.19. The rate constants for reactions in the recovery process in DMSO are shown in Table 4.20.

The recovery process comprises three reaction steps, **17 → TS8 → 18**, **18 → 19** and **19 → Cat + Cl₂**. This process is the chlorination of the chlorinated Cu–pillared clay catalyst and affords chlorine gas and clean Cu–pillared clay catalyst. The structure optimizations for the Cu–pillared clay catalyst complexes interacting with CCl_4 namely the species of **17**, **TS8** and **18** (Figure 4.31), the quartet spin state being used. The spin states and spin contaminations for all related species are listed in Table A-6.
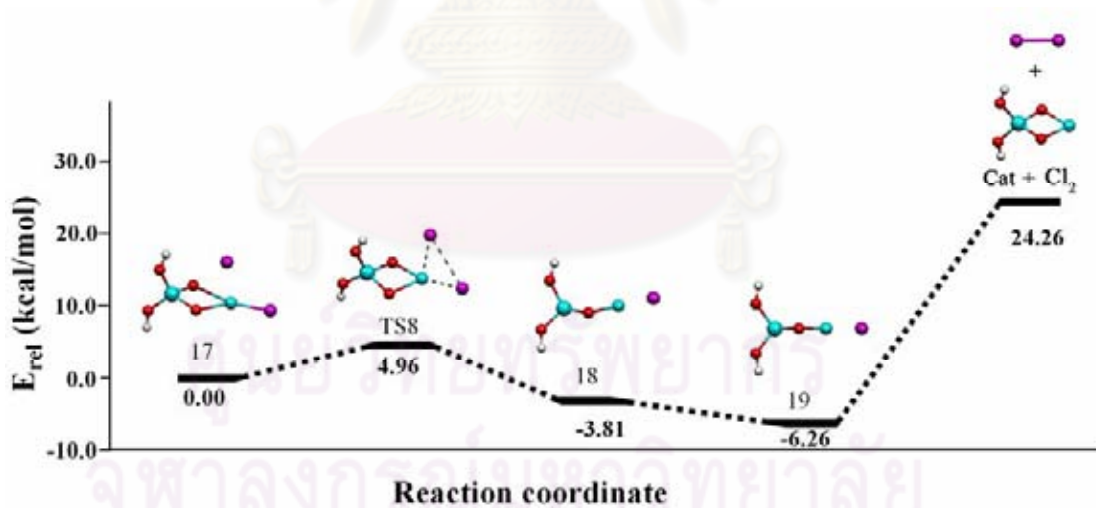
Figure 4.31 Potential energy profile for the recovery process of Cu–pillared clay catalyst.
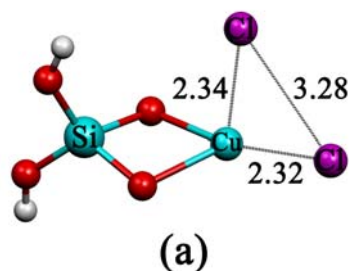
Figure 4.32 The transition–state structures for recovery process (a) TS8 were optimized at B3LYP/LanL2DZ levels of theory. Bond distances are in Å.

Table 4.18 Imaginary frequencies for transition states of the recovery process

transition state	imaginary frequency, cm^{-1}
TS8	−124.55

Table 4.19 Reaction energies, thermodynamic properties, rate and equilibrium constants for the recovery process of Cu–pillared clay catalyst, in gas phase

Reaction	$\Delta^{\ddagger}E$ [a,b]	$\Delta^{\ddagger}G$ [a,b]	k_{298} [c]	ΔE [a]	ΔH_{298} [a]	ΔG_{298} [a]	K_{298}
Recovery process :							
$17 \rightarrow TS8 \rightarrow 18$	4.96	− 3.86	9.97×10^8	− 3.81	− 3.82	− 3.86	6.79×10^2
$18 \rightarrow 19$	−	− 1.14	−	− 2.45	− 2.84	− 1.14	6.88×10^0
$19 \rightarrow Cat^e + Cl_2$	−	21.06	−	30.52	30.03	21.06	3.66×10^{-16}

[a] In kcal/mol.

[b] Activation state.

[c] Computed using Eq. 2.28, in s^{-1}.

[e] Cu–pillared clay catalyst.

Table 4.20 Reaction energies, Gibbs free energies, rate and equilibrium constants for the recovery process of the Cu–pillared clay catalyst in DMSO

Reaction	$\Delta\Delta^{\ddagger}G$ [a,b,c]	k_{298} [d]	$\Delta\Delta G_{298}$ [a,c]	K_{298}
Recovery process :				
$17^{e} \rightarrow TS8 \rightarrow 18$	5.80	3.48×10^{8}	4.36	1.57×10^{3}
$18 \rightarrow 19$	–	–	–3.45	3.37×10^{2}
$19 \rightarrow 6^{f} + Cl_2$	–	–	25.80	1.22×10^{-19}

[a] In kcal/mol.

[b] Activation state.

[c] In DMSO, derived from the single–point CPCM calculation (ε=46.7) at the B3LYP/LanL2DZ level.

[d] Computed using Eq. (2.26), in s^{-1}.

[e] The complex of the di–chlorinated Cu–pillared clay catalyst

[f] Cu–pillared clay catalyst.

Table 4.19 shows that free energy of reaction steps **17 → TS8 → 18** and **18 → 19** is spontaneous reaction in gas phase. The reaction steps **17 → TS8 → 18** and **18 → 19** are found to be an exothermic reaction. The rate constant of **17 → TS8 → 18**, $9.97 \times 10^{8} \, s^{-1}$ was obtained. Activation energies, tunneling coefficients, A factors and rate constants of reactions in the recovery process of Cu–pillared clay catalyst are shown in Table 4.21. The pre–exponential parameters (κ.A) are acceptable values as compared with any exponential results.

Table 4.21 Activation energies, tunneling coefficients, A factors and rate constants of reactions in the recovery process of Cu–pillared clay catalyst, computed at the B3LYP/LanL2DZ in gas phase

Reaction	κ^a	Q_{TS}/Q_{REA}	A^b	$\Delta^{\ddagger}E^c$	$k_{298}{}^d$
Dechlorination :					
$17 \to TS8 \to 18$	1.02	6.81×10^{-1}	4.23×10^{12}	4.96	9.97×10^8
$18 \to 19$	–	–	–	–	–
$19 \to Cat^e + Cl_2$	–	–	–	–	–

^{a} $\kappa = 1 + \dfrac{1}{24}\left(\dfrac{h\nu_i}{k_B T}\right)^2$.

^{b} $A = \dfrac{k_B T}{h}\dfrac{Q_{TS}}{Q_{REA}}$, in s^{-1}.

^{c} Computed with ZPVE corrections, in kcal/mol.

^{d} Computed using Eq. 2.28, in s^{-1}.
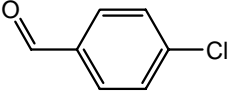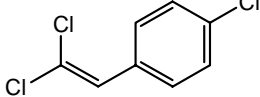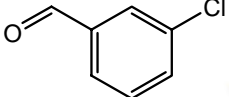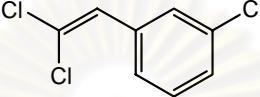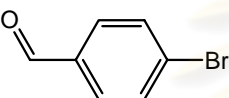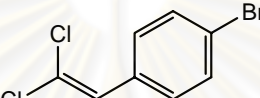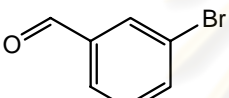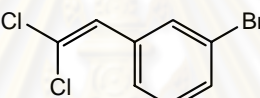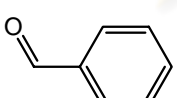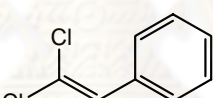
^{e} Cu–pillared clay catalyst.

4.7 Comparison of olefinations for all synthetic products

Rate constants and Gibbs free energies for olefination reactions of all synthetic systems based on rate–determining step are shown in Table 4.22. It shows that different position of substituents of halogenobenzaldehyde compounds hardly affect the reaction rate. We can conclude that these rate constants based on rate–determining step for all olefinations are in the same order of magnitude. From the experimental results of the syntheses of halogenobenzaldehyde compounds, the same amount of their percent yields were found except the synthesis of DCVB as shown in Table 4.22. It may be caused by the poor model of copper pillared catalyst being used in the calculation. The structure micro/mesoporous character of pillared layer has not been included in catalyst model for using in the calculations.

The reaction mechanisms of the syntheses of halogenobenzaldehyde compounds obtained in this work are composed of four reaction processes which are similar to the mechanism proposed by Nenaidenko *et al*. [1]. Nevertheless, the reaction mechanisms obtained in this work contain many reaction steps as compared to the mechanism proposed by Nenaidenko.

Table 4.22 Rate constants based on rate–determining step for olefinations of all reactants and their corresponding Gibbs free energies at activation

Entry	Reactants	Products	k_{RDS}[c]	$\Delta^{\ddagger}G$[a,b]	% yield[48]
1			2.09×10^{-52}	88.48	72
2			1.52×10^{-52}	88.67	53
3			2.04×10^{-52}	88.50	69
4			2.61×10^{-52}	88.35	60
5			2.71×10^{-52}	88.31	25

[a] In kcal/mol.

[b] Gibbs free energy at activation.

[c] Computed using Eq. 2.28, in s^{-1}.

CHAPTER V

CONCLUSIONS

In the present study, theoretical investigations on reaction mechanisms of olefinations of 4–chlorobenzaldehyde (4CBD), 3–chlorobenzaldehyde (3CBD), 4–bromobenzaldehyde (4BBD), 3–bromobenzaldehyde (3BBD) and benzaldehyde (BD) with hydrazine and carbontetrachloride (CCl_4) to yeild 1–(2,2–dichlorovinyl)–4–chlorobenzene (DCV4CB), 1–(2,2–dichlorovinyl)–3–chlorobenzene (DCV3CB), 1–(2,2–dichlorovinyl)–4–bromobenzene (DCV4BB), 1–(2,2–dichlorovinyl)–3–bromobenzene (DCV3BB) and 1–(2,2–dichlorovinyl)–benzene (DCVB), respectively catalyzed by copper oxide–pillared clay using the B3LYP/LanL2DZ method were carried out. All the studied results are concluded as the following issues:

- The mechanism of all olefinations are composed of four reaction processes namely (i) precursor formation, (ii) dehydrodenitrogenation (iii) chlorination and (iv) recovery process.

- Rate–determining steps of the studied reactions are the same reaction step, [**5**···**6**] → **TS3** → [**7**···**8**].

- Rate constants due to rate–determining step of olefinations to yeild the DCV4CB, DCV3CB, DCV4BB, DCV3BB and DCVB products are 2.09×10^{-52} s^{-1}, 1.52×10^{-52} s^{-1}, 2.04×10^{-52} s^{-1}, 2.61×10^{-52} s^{-1} and 2.71×10^{-52} s^{-1}, respectively.

- The reaction mechanisms of conversion of 4CBD to DCV4CB in gas phase and in DMSO are in the similar manner.

Suggestion for future work

The reaction mechanism of olefination using various transition metal ions exchanged–pillared clay catalysts should be investigated in order to obtain high conversion of alkene products. The Cu–pillared clay catalyst model used in this study should be replaced with the larger cluster models including the periodic model.

REFERENCES

[1]   Nenajdenko V.G.; Korotchenk V.N.; Shastin A.V.; Tyurin D.A.; Balenkova
        E.S. Catalytic Olefination Estimation of the Reactivity of
        Polyhaloalkanes. *Russ. J. Org. Chem*. 40 (2003): 1750-1756.

[2]   Nenajdenko V.G.; Varseev G.N.; Korotchenko V.N.; Shastin A.V.; Balenkova
        E.S. Reaction of $CBrF_2$–$CBrF_2$ with hydrazones of aromatic aldehydes
        Novel efficient synthesis of fluorocontaining alkanes, alkenes and
        alkynes. *J. Fluor. Chem*. 125 (2004): 1339-1345.

[3]   Nenajdenko V.G.; Varseev G.N.; Korotchenko V.N.; Shastin A.V.; Balenkova
        E.S. A novel direct synthesis of (2,2-difluorovinyl)benzenes from
        aromatic aldehydes. *J. Fluor. Chem*. 124 (2003): 115-118.

[4]   Nenajdenko V.G.; Varseev G.N.; Shastin A.V.; Balenkova E.S. The catalytic
        olefination reaction of aldehydes and ketones with CBr_3CF_3. *J. Fluor.
        Chem*. 126 (2005): 907-913.

[5]   Nenajdenko V.G.; Shastin A.V.; Korotchenko V.N.; Balenkova, E.S.
        Conversion of aromatic aldehydes into 1-aryl-2,2-dichloroethenes. *Rus.
        Chem. Bull*. 50 (2001): 1047-1050.

[6]   Shichi T.; Takagi K. Clay Minerals as Photochemical reaction fields. *J.
        Photochem. Photobiol*. (2000): 113-130.

[7]   Moore D.M.; Reynolds R.C. X-ray Diffraction and the Identification and
        Analysis of Clay Minerals. *New York, USA, Oxford University Press*,
        (1989): 256.

[8]   Bruce, W.D.; O' Hare, D. *Inorganic Material*. 2nd edition. New York: John
        Wiley and Sons, 1997.

[9]   Vicente M.A.; Belver C.; Trujillano R.; Banares-Munos M.A.; Rives V.;
        Korili S.A.; Gil A.; Gandia L.M.; Lambert J.F. Preparation and
        characterisation of vanadium catalysts supported over alumina-pillared
        clays. *Catal. Today*. 78 (2003): 181-182.

[10]   Robert A.S.; Tom P.; Gerhard L.; Nick G. Pillared Clay and Pillared Layered
        Solids. *Pure Appl. Chem*. 71 (1999): 2367-2371.

[11] Ozen C.; Tuzun S.N. A DFT Study on the Machanism of Cyclopropanation via Cu(aca)$_2$-Catalyzed Diazo Ester Decomposition. *Organomet*. 27 (2008): 4600-4610.

[12] Davi M.; Lebel H. Copper-Catalyzed Tandem Oxidation-Olefination Process. *Org. Lett*. 11(2009): 41-44.

[13] Lin Y.; Li Z.; Casarotto V.; Ehrmantraut J.; Nguyen A.N. A catalytic, highly stereoselective aldehyde olefination reaction. *Tetra. Lett*. 48 (2007): 5531-5534.

[14] Jean F.L.; Georges P. Acidity in Pillared Clays. Origin and Catalytic Manigestation. *Top. Catal. 4*, 43 (1997): 34-46.

[15] Francisco R.; Valenzuela D.; Santos P.S. Studies on the Acid Activation of Brazilian Smectitic Clays. *Quim. Nova*. 24 (2001): 345-353.

[16] Gonzalez F.; Pesquera C.; Blanco C.; Benito I.; Mendioroz S. Synthesis and Characterization of Al-Ga Pillared Clays with High Thermal and Hydrothermal Stability. *Inorg. Chem*., 31 (1992): 727-733.

[17] Chatterjee A.; Iwasaki T.; Ebina T.; Miyamoto A. A DFT study on clay-cation-water intersction in montmorillonite and beidellite. *Comput. Mate. Sci*. 14 (1999): 119-124.

[18] Shastin A.V.; Muzalevskii V.M.; Korotchenko V.N.; Balenkova E.S.; Nenajdenko, V.G. Effect of Catalyst Nature and Quantity on Catalytic Olefination. *Russ. J. Org. Chem*. 42 (2006): 183-189.

[19] Joseph T.; Shanbhag G.V.; Halligudi S.B. Copper(II) Ion-exchanged Montmorillonite as Catalyst for the Direct Addition of N-H Bond to CC Tiple Bond. *J. Mol .Catal*. 236 (2005): 139-144.

[20] An Z.; Zhang J.; Wang R.; Koga N. DFT investigation for 1:2 complexes of bis(hexafluoroacetonato)copper(II) coordinated with 4-(*N-tert*-bulyl-*N*-oxyamino)pyridine. *Polyhedron*. 26(2007): 2126-2128.

[21] Lewars E. Computational chemistry. *Canada: Trent University*, 2003.

[22] Grant, G.H.; Richards, W.G. Computational chemistry. New York: Oxford university press, 1995.

[23] Davidson E.R.; Feller D. Basis set selection for molecular calculations. *J. Chem. Rev*. 86(1986): 681-696.

[24] Huang H.Y.; Padin J.; Yang R.T. Anion and Cation Effects on Olefin Adsorption on Silver and Copper Halides: Ab Initio Effective Core Potential Study of ∂-Complexation. *J. Phys. Chem. B* 103 (1999): 3206–3212.

[25] Hirschfelder J.O.; Wigner E. Some quantum-mechanical considerations in the theory of reactions involving an activation energy. *J. Chem. Phys.* 7 (1939): 616-628.

[26] Eckart C. The Penetration of a Potential Barrier by Electrons. *Phys. Rev.* 35 (1930): 1303-1309.

[27] Garrett, B.C.; Truhlar, D.G.; Grev, R.S.; Magnuson, A.W. Improved treatment of threshold contributions in variational transition-state theory. *J. Phys. Chem.* 84 (1980): 1730-1748.

[28] Skodje, R.T.; Truhlar, D.G.; Garrett, B.C. A general small-curvature approximation for transition-state-theory transmission coefficients. *J. Phys. Chem.* 85 (1981): 3019-3023.

[29] Cramer, C.J. Essentials of computational chemistry: theories and models, 2nd edition. Singapore: John Wiley and Sons, 2004.

[30] Ochterski, J.W. Thermochemistry in Gaussian, Gaussian Inc., Wallingford, CT, 2000.

[31] Curtiss L.A.; Raghavachari K.; Redfern P.C.; Pople J.A. Assessment of Gaussian-2 and density functional theories for the computation of enthalpies of formation. *Chem. Phys.* 106 (1997): 1063-1079.

[32] Becke A.D. Density-functional thermochemistry. III. The role of exact exchange. *J. Chem. Phys.*, 98 (1993): 5648-5652.

[33] Lee C.; Yang W.; Parr R.G. Development of the Colle-Salvetti correlation-energy formula into a functional of the electron density. *Phys. Rev. B* 37 (1988): 785–789.

[34] Hay P.J.; Wadt W.R. Ab initio effective core potentials for molecular calculations: potentials for the transition metal atom Sc to Hg. *J. Chem. Phys.* 82 (1985): 270–283.

[35] Wadt W.R.; Hay P.J. Ab initio effective core potentials for molecular calculations: potentials for main group elements Na to Bi. *J. Chem. Phys.* 82 (1985): 284–298.

[36]   Hay P.J.; Wadt W.R. Ab initio effective core potentials for molecular calculations: potentials for K to Au including the outermost core orbitals. *J. Chem. Phys*. 82 (1985): 299–310.

[37]   Peng C.; Ayala P.Y.; Schlegel H.B.; Frisch M.J. Using redundant internal coordinates to optimize geometries and transition states. *J. Comp. Chem*. 17 (1996): 49–56.

[38]   Gonzalez C.; Schlegel H.B. An Improved Algorithm for Reaction Path Following. *J. Chem. Phys*., 90 (1989): 2154–2161.

[39]   Barone V.; Cossi M. Quantum calculation of molecular energies and energy gradients in solution by a conductor solvent model. *J. Phys. Chem. A* 102 (1998): 1995-2001.

[40]   Barone V.; Cossi M.; Tomai J. Geometry optimization of molecular structures in solution by the polarizable continuum model. *J. Comput. Chem*. 19 (1998): 404-417.

[41]   Cossi M.T.; Barone V.; Mennucci B.; Tomasi J. Ab initio study of ionic solutions by a polarizable continuum dielectric model. *Chem. Phys. Lett*. 286 (1998): 253-260.

[42]   Cances M.T.; Mennucci V.; Tomasi J. A new integral equation formalism for the polarizable continuum model: Theoretical background and applications to Isotropic and anisotropic dielectrics. *J. Chem. Phys*. 107 (1997): 3032-3041.

[43]   Barone V.; Cossi M.; Mennucci B.; Tomasi J. A new definition of cavities for the computation of solvation free energies by the polarizable continuum model. *J. Chem. Phys*. 107 (1997): 3210-3221.

[44]   Cossi M.; Barone V.; Cammi R.; Tomasi J. Ab initio study of solvated molecules: A new implementation of the polarizable continuum model. *Chem. Phys. Lett*., 255 (1996): 327-335.

[45]   Miertus S.; Tomasi J. Approximate evaluations of the electrostatic free energy and internal energy changes in solution processes. *Chem. Phys*. 65 (1982): 239-245.

[46]   Frisch M.J. et al. GAUSSIAN 03. Revision D.02, Gaussian Inc., Wallingford, CT, 2004.

[47]   Bravo–Perez G.; Alvarez–Idaboy J. R.; Cruz–Torres A.; . Ruiz M. E. Quantum
         chemical and conventional transition-state theory calculations of rate
         constants for the NO_3 alkane reaction. *J. Phys. Chem. A* 106 (2002):
         4645-4650.

[48]   Rojtinnakorn K. Olefination of carbonyl compounds catalyzed by copper
         oxide-pillared clay. Master's Thesis, Program in Petrochemistry and
         Polymerscience Faculty of Science, Chulalongkorn University 2007.

APPENDICES

APPENDIX A

Table A-1 The spin contaminations, S^2 for all related species of olefination reaction for synthesis of the DCV4CB product in gas phase, computed at the B3LYP/LanL2DZ level of theory

Species	$S^{2\,a}$	
	Theoretical value [b]	Computational value
1A	0.0000	0.0000
HZ	0.0000	0.0000
[1A···HZ]	0.0000	0.0000
TS1_A	0.0000	0.0000
3A	0.0000	0.0000
TS2_A	0.0000	0.0000
[W···5A]	0.0000	0.0000
W	0.0000	0.0000
5A	0.0000	0.0000
Cat	0.7500	0.7500
[5A···Cat]	0.7500	0.7500
TS3_A	0.7500	0.7501
[H_2···8A]	0.7500	0.7501
H_2	0.0000	0.0000
8A	0.7500	0.7501
TS4_A	0.7500	0.7500
9A	0.7500	0.7500
TS5_A	0.7500	0.7525
[N_2···11A]	0.7500	0.7500
N_2	0.7500	0.7500
11A	0.7500	0.7501
CCl_4	0.0000	0.0000
[11A···CCl_4]	0.7500	0.7500
TS6_A	3.7500	3.7502
13A	3.7500	3.7502
TS7_A	3.7500	3.7503
14A	3.7500	3.7504
15A	3.7500	3.7502

[a] Spin contaminant, $S^2 = S(S+1)$.

[b] Spin for S^2=0.0000 is S =0, S^2=0.7500 is S =1/2 and S^2=3.7500 is S =3/2.

Table A-2 The spin contaminations, S^2 for all related species of olefination reaction for synthesis of the DCV3CB product in gas phase, computed at the B3LYP/LanL2DZ level of theory

Species	$S^{2\,a}$	
	Theoretical value [b]	Computational value
1B	0.0000	0.0000
HZ	0.0000	0.0000
[1B···HZ]	0.0000	0.0000
TS1_B	0.0000	0.0000
3B	0.0000	0.0000
TS2_B	0.0000	0.0000
[W···5B]	0.0000	0.0000
W	0.0000	0.0000
5B	0.0000	0.0000
Cat	0.7500	0.7500
[5B···Cat]	0.7500	0.7500
TS3_B	0.7500	0.7501
[H_2···8B]	0.7500	0.7501
H_2	0.0000	0.0000
8B	0.7500	0.7501
TS4_B	0.7500	0.7500
9B	0.7500	0.7500
TS5_B	0.7500	0.7527
[N_2···11B]	0.7500	0.7501
N_2	0.7500	0.0000
11B	0.7500	0.7501
CCl_4	0.0000	0.0000
[11B···CCl_4]	0.7500	0.7501
TS6_B	3.7500	3.7502
13B	3.7500	3.7502
TS7_B	3.7500	3.7503
14B	3.7500	3.7505
15B	3.7500	3.7502

[a] Spin contaminant, $S^2 = S(S+1)$.

[b] Spin for S^2=0.00 is S =0, S^2=0.75 is S =1/2 and S^2=3.75 is S =3/2.

Table A-3 The spin contaminations, S^2 for all related species of olefination reaction for synthesis of the DCV4BB product in gas phase, computed at the B3LYP/LanL2DZ level of theory

Species	$S^{2\,a}$	
	Theoretical value [b]	Computational value
1C	0.0000	0.0000
HZ	0.0000	0.0000
[1C···HZ]	0.0000	0.0000
TS1_C	0.0000	0.0000
3C	0.0000	0.0000
TS2_C	0.0000	0.0000
[W···5C]	0.0000	0.0000
W	0.0000	0.0000
5C	0.0000	0.0000
Cat	0.7500	0.7500
[5C···Cat]	0.7500	0.7500
TS3_C	0.7500	0.7501
[H$_2$···8A]	0.7500	0.7501
H$_2$	0.0000	0.0000
8C	0.7500	0.7501
TS4_C	0.7500	0.7500
9C	0.7500	0.7500
TS5_C	0.7500	0.7525
[N$_2$···11C]	0.7500	0.7500
N$_2$	0.7500	0.0000
11C	0.7500	0.7501
CCl$_4$	0.0000	0.0000
[11C···CCl$_4$]	0.7500	0.7500
TS6_C	3.7500	3.7502
13C	3.7500	3.7502
TS7_C	3.7500	3.7503
14C	3.7500	3.7505
15C	3.7500	3.7502

[a] Spin contaminant, $S^2 = S(S+1)$.

[b] Spin for S^2=0.00 is S=0, S^2=0.75 is S=1/2 and S^2=3.75 is S=3/2.

Table A-4 The spin contaminations, S^2 for all related species of olefination reaction for synthesis of the DCV3BB product in gas phase, computed at the B3LYP/LanL2DZ level of theory

Species	$S^{2\,a}$	
	Theoretical value [b]	Computational value
1D	0.0000	0.0000
HZ	0.0000	0.0000
[1D···HZ]	0.0000	0.0000
TS1_D	0.0000	0.0000
3D	0.0000	0.0000
TS2_D	0.0000	0.0000
[W···5D]	0.0000	0.0000
W	0.0000	0.0000
5D	0.0000	0.0000
Cat	0.7500	0.7500
[5D···Cat]	0.7500	0.7500
TS3_D	0.7500	0.7501
[H_2···8D]	0.7500	0.7501
H_2	0.0000	0.0000
8D	0.7500	0.7501
TS4_D	0.7500	0.7500
9D	0.7500	0.7500
TS5_D	0.7500	0.7527
[N_2···11D]	0.7500	0.7500
N_2	0.7500	0.0000
11D	0.7500	0.7501
CCl_4	0.0000	0.0000
[11D···CCl_4]	0.7500	0.7501
TS6_D	3.7500	3.7502
13D	3.7500	3.7502
TS7_D	3.7500	3.7503
14D	3.7500	3.7505
15D	3.7500	3.7502

[a] Spin contaminant, $S^2 = S(S+1)$.

[b] Spin for S^2=0.00 is S =0, S^2=0.75 is S =1/2 and S^2=3.75 is S =3/2.

Table A-5 The spin contaminations, S^2 for all related species of olefination reaction for synthesis of the DCVB product in gas phase, computed at the B3LYP/LanL2DZ level of theory

Species	$S^{2\,a}$	
	Theoretical value [b]	Computational value
1E	0.0000	0.0000
HZ	0.0000	0.0000
[1E···HZ]	0.0000	0.0000
TS1_E	0.0000	0.0000
3E	0.0000	0.0000
TS2_E	0.0000	0.0000
[W···5E]	0.0000	0.0000
W	0.0000	0.0000
5E	0.0000	0.0000
Cat	0.7500	0.7500
[5E···Cat]	0.7500	0.7500
TS3_E	0.7500	0.7501
[H_2···8E]	0.7500	0.7501
H_2	0.0000	0.0000
8E	0.7500	0.7501
TS4_E	0.7500	0.7500
9E	0.7500	0.7500
TS5_E	0.7500	0.7523
[N_2···11E]	0.7500	0.7500
N_2	0.7500	0.0000
11E	0.7500	0.7501
CCl_4	0.0000	0.0000
[11E···CCl_4]	0.7500	0.7500
TS6_E	3.7500	3.7502
13E	3.7500	3.7502
TS7_E	3.7500	3.7503
14E	3.7500	3.7505
15E	3.7500	3.7502

[a] Spin contaminant, $S^2 = S(S+1)$.

[b] Spin for S^2=0.00 is S =0, S^2=0.75 is S =1/2 and S^2=3.75 is S =3/2.

Table A-6 The spin contaminations, S^2 for all related species of olefination reaction for recovery process of the Cu–pillared clay catalyst in gas phase, computed at the B3LYP/LanL2DZ level of theory

Species	$S^{2\,a}$	
	Theoretical value [b]	Computational value
17	3.7500	3.7501
TS8	3.7500	3.7501
18	3.7500	3.7501
19	0.7500	0.7500
Cat	0.7500	0.7500
Cl_2	0.0000	0.0000

[a] Spin contaminant, $S^2 = S(S+1)$.

[b] Spin for S^2=0.00 is S=0, S^2=0.75 is S=1/2 and S^2=3.75 is S=3/2.

VITA

Name:	Miss LALITA NAMMUENG
Date of Birth:	March 14th, 1985
Place of Birth:	Phetchabun, Thailand
Address:	80 M.2 T. Yangrak, Khokcharoen, Lopburi 15250, Thailand
Telephone:	086-5530290
E-mail address:	lalita_1414@hotmail.com

Educations:

2008-2010   M.Sc. (Petrochemistry and Polymer Science), Chulalongkorn University, Thailand

2003-2007   B.Eng. (Petrochemical and Polymeric Materials), Silpakorn University, Thailand

2000-2002   Pranarai high school, Lopburi, Thailand

1997-1999   Yangrak wittaya secondary school, Lopburi, Thailand

1991-1996   Banyangrak primary school, Lopburi, Thailand

Scholarship:

2009-2010   The NCE-PPAM (National Center of Excellence for Petroleum, Petrochemicals and Advanced Materials)

Presentation:

2010   Lalita Nammueng, Nipaka Sukpirom, Vithaya Ruangpornvisuti, Theoretical study of olefination reaction of carbonyl compounds catalyzed by copper oxide-pillared Montmorillonite (Poster Session): Joint conference of 7th International Symposium on Advanced Materials in Asia-Pacific (7thISAMAP) and JAIST International Symposium on Nano Technology 2010 (NT2010), 30 September-1October 2010. Asahidai, Nomi, Ishikawa, Japan

2010   Lalita Nammueng, Nipaka Sukpirom, Vithaya Ruangpornvisuti, Theoretical study of olefination reaction of carbonyl compounds catalyzed by copper oxide-pillared clay (Poster Session): 3rd Silpakorn University Research Fair on Creative Economy Conference, 28-29 January 2009. Silpakorn University, Nakhonpathom, Thailand